Loss of non-canonical KCC2 functions promotes developmental apoptosis of cortical projection neurons

Martina Mavrovic[1,2], Pavel Uvarov[1,2], Eric Delpire[3], Laszlo Vutskits[4,5], Kai Kaila[1,2], Martin Puskarjov[1¤]*

[1]Molecular and Integrative Biosciences, University of Helsinki, 00014 Helsinki, Finland

[2]Neuroscience Center, Helsinki Institute of Life Science, University of Helsinki, 00014 Helsinki, Finland

[3]Department of Anesthesiology, Vanderbilt University Department of Anesthesiology, Vanderbilt University, Nashville, TN 37232, USA

[4]Department of Basic Neurosciences, University of Geneva Medical School, 1211 Geneva 4, Switzerland

[5]Department of Anesthesiology, Pharmacology, Intensive Care and Emergency Medicine, University Hospitals of Geneva, 1211 Geneva 4, Switzerland

*Correspondence: Martin.Puskarjov@Helsinki.fi

[¤]Lead contact

ABSTRACT

KCC2, encoded in humans by the *SLC12A5* gene, is a multifunctional neuron-specific protein initially identified as the chloride (Cl^-) extruder critical for hyperpolarizing $GABA_A$ receptor currents. Independently of its canonical function as a K-Cl cotransporter, KCC2 regulates the actin cytoskeleton via molecular interactions mediated through its large intracellular C-terminal domain (CTD). Contrary to the common assumption that embryonic neocortical projection neurons express KCC2 at non-significant levels, here we show that loss of KCC2 enhances apoptosis of late-born upper layer cortical projection neurons. *In utero* electroporation of plasmids encoding truncated, transport-dead KCC2 constructs retaining the CTD were as efficient as those encoding full-length KCC2 in preventing elimination of migrating projection neurons upon conditional deletion of KCC2. This was in contrast to the effect of a full-length KCC2 construct bearing a CTD missense mutation ($KCC2^{R952H}$), which disrupts cytoskeletal interactions and has been found in patients with neurological and psychiatric disorders, notably seizures and epilepsy. Together, our findings indicate an ion-transport independent, CTD-mediated regulation of developmental apoptosis by KCC2 in migrating cortical projection neurons.

Keywords: cell death, migration, GABA, chloride, cofilin, KCC2

INTRODUCTION

During early cortical development, neurons are generated in excess, and a substantial portion of them undergo apoptosis, a process crucial for the establishment of the final number of neurons and the organization of cerebrocortical networks [1–3]. In the mouse neocortex, the first wave of apoptosis affects neural progenitors and early post-mitotic neurons during embryonic development, with a peak around embryonic day (E) 14 [3–5]. This roughly corresponds to the first apoptotic wave in humans from the postconceptional week (PCW) 6.5 up until the end of the first trimester of gestation [6,7]. The second peak in developmental neuroapoptosis is activity-dependent and takes place during the first postnatal week in the mouse, this time affecting newly differentiated neurons [8–10]. Ultimately, up to 40% of cortical neurons are eliminated by developmental apoptosis [11,12]. Some neuronal populations, like the Cajal-

Retzius neurons (CRNs), disappear almost entirely during the second wave of apoptosis [13,14]. Contrary to the overall cortical neuronal population, CRNs do not show developmental up-regulation of the neuronal K-Cl cotransporter KCC2, but persistently express the Cl^- importer NKCC1, resulting in excitation of CRNs by $GABA_A$ receptors ($GABA_A$Rs) [15,16]. Interestingly, reduction of intracellular Cl^- by genetic deletion of NKCC1 or its inhibition with bumetanide exerts a pro-survival effect on these cells *in vitro* [17].

$GABA_A$R activation during embryonic development elicits depolarizing or even excitatory actions on CNS neurons, which play an important role in neuronal proliferation, migration, and synaptogenesis [18,19]. The developmental increase in Cl^- extrusion mediated by KCC2 sets the low intraneuronal Cl^- concentration needed for hyperpolarizing $GABA_A$R-mediated signaling in most mature central neurons [20,21]. At the time of the first apoptotic wave, synaptic coupling of cortical neurons is however relatively weak [22–24], and neuroapoptosis at this early stage is likely to be independent of neuronal activity.

Genetic ablation of KCC2 in mature hippocampal pyramidal neurons has been reported to decrease their survival [25,26]. In contrast, ablation of KCC2 in migrating cortical interneurons did not alter their rate of apoptosis, despite early expression of KCC2 in this type of neuron [27]. Contrary to the widespread assumption that KCC2 is expressed at a non-significant level in perinatal mouse and rat cortical pyramidal neurons, we recently found that KCC2-mediated Cl^- extrusion in hippocampal CA3 pyramidal neurons exerts significant control over spontaneous network events already at this early stage in development [28]. It is, however, unknown what role KCC2 may play in migrating neocortical projection neurons (PNs) in which KCC2, upon overexpression, appears to be kinetically inactivated as an ion transporter until around birth in altricial rodents [29,30].

Independently of its canonical K-Cl cotransport function, KCC2 also regulates the actin cytoskeleton in dendritic spines via interactions mediated by its C-terminal domain (CTD) [31–35]. This is in part achieved by modulating the phosphorylation of cofilin, one of the major actin-regulating proteins [36,37]. KCC2 mutations found in patients with neurodevelopmental disorders [38–40] may disrupt both ion transport-dependent and transport-independent functions of KCC2, prompting the idea that alterations in KCC2 expression unrelated to chloride regulation may have clinically important consequences on neuronal development [38].

Here we show using constitutive and conditional knockout models that loss of the non-canonical ion transport-independent functions of KCC2 in late-born upper layer cortical projection neurons promotes their developmental apoptosis *in vivo*. Our data indicate that signalling mediated by the KCC2 CTD is involved in the timely elimination of projection neurons during neurogenesis.

RESULTS AND DISCUSSION

Genetic loss of KCC2 promotes apoptosis of embryonic neocortical projection neurons *in vivo*

In contrast to the well-characterized postnatal up-regulation of KCC2 in neocortical PNs of mice and rats [20,35,41–44], little information is available on expression patterns of KCC2 in perinatal, migrating neocortical PNs. To explore the temporal expression of KCC2 in embryonic mouse neocortical PNs, we used the Developing Cortical Neuron Transcriptome RNA-seq resource ([45];Data ref: [46]). In line with previous work on the expression levels of KCC2 protein in E15.5 mouse cortex [47], mRNA encoding KCC2 (*Slc12a5*) was expressed at a detectable level (FPKM ≥ 2; [45]; Data ref: [46]) on E15.5, E16.5 and E18.5 in subcerebral (FPKM, E15.5: 3.4 ± 1.1; E16.5: 8.0 ± 2.3; E18.5: 18.5 ± 4.8), corticothalamic (FPKM, E15.5: 5.1 ± 1.7; E16.5: 7.5 ± 2.1; E18.5: 19.4 ± 5.3), and callosal PNs (FPKM, E15.5: 2.9 ± 1.0; E16.5: 2.3 ± 0.8; E18.5: 9.6 ± 2.8) (Fig EV1).

We next explored whether and how the deletion of endogenous KCC2 may affect the development of immature pyramidal neurons in the embryonic mouse cortex. To this end, we generated a *Kcc2*$^{lox/lox}$ mouse, in which exon-5 is flanked by loxP sites. Deleting exon-5 results in a frameshift and a preterm stop codon,

thus abolishing KCC2 expression (Fig EV2A). Successful deletion of this exon upon expression of Cre-recombinase (Cre) was verified by crossing these mice with E2a-CRE deleter mice (Fig EV2B), or by transfecting primary cortical neurons with Cre (Fig EV2C).

To follow KCC2 expression at E18.5 in PNs migrating to the upper cortical layers, we used *in utero* electroporation (IUE) of an EGFP construct in *Kcc2*$^{lox/lox}$ embryos at E14.5. At this age, IUE targets neural progenitors that give rise to the initial migratory wave of layer II/III PNs and to the last wave of layer IV upper cortical PNs [48]. IUE was carried out using the classical 0° electrode paddle orientation [49], which enables selective targeting of PNs with no effect on interneuronal progenitors [50,51]. KCC2 immunostaining using an anti-KCC2 antibody validated in E18.5 *Kcc2*$^{-/-}$ cortical sections [28], revealed that a fraction (14.5 ± 1.2%) of EGFP^{+} neurons in the cortical plate had somatic, plasmalemmal-like KCC2 immunoreactivity (Fig EV2D and E). The fraction of neurons with such an immunosignal at E18.5 among the upper cortical PNs labeled with IUE of EGFP at 14.5 observed presently is close to the 13-30% reported for hippocampal CA3 pyramidal neurons at this age [28,52]. These are, however, likely to be underestimates as a substantial part of the total KCC2 pool may be contained in transport vesicles [52–54], where the CTD of KCC2 is facing the cytosol and free to interact with its targets.

To delete KCC2 from a sub-population of PNs destined for upper cortical layers, we employed IUE of plasmids expressing Cre and a fluorescent marker (EGFP or RFP) in *Kcc2*$^{lox/lox}$ embryos. The efficacy of Cre-mediated ablation of KCC2 in *Kcc2*$^{lox/lox}$ animals at E18.5 was confirmed using KCC2 immunostaining, which showed that 0.3 ± 0.1% of the neurons co-electroporated with EGFP and Cre (EGFP+Cre) were KCC2^{+} (Fig EV2D and E). Analysis of Cre immunostaining showed co-expression of Cre in the vast majority of EGFP^{+} neurons (Fig EV2F and G), in line with our previous results on the high level of co-expression of plasmid constructs following co-electroporation *in utero* [34].

Previous studies reported no effect of KCC2 overexpression in layer II-IV PN progenitors on the distribution (reflecting both proliferation and migration) of the derived PNs in the embryonic cortex [29,55]. Given that genetic ablation of KCC2 in mature hippocampal pyramidal neurons has been reported to decrease their survival [25,26], we compared the number of EGFP^{+} neurons/region of interest (ROI) at E18.5 in slices prepared from embryos co-electroporated with EGFP+Cre to the controls electroporated with EGFP alone at E14.5. A significantly fewer number of neurons was observed in *Kcc2*$^{lox/lox}$ embryos co-electroporated with Cre (-57.4 ± 6.7% to EGFP; Fig 1A and B). The number of neurons co-electroporated with Cre and a plasmid encoding full-length KCC2 (KCC2^{FL}; [31,34,44]) was not different from control (-3.59 ± 9.9% to EGFP; Fig 1A and B), indicating that the Cre-induced decrease in the number of EGFP^{+} *Kcc2*$^{lox/lox}$ neurons could be prevented by compensating for the loss of endogenous KCC2. The same effect of Cre was observed when EGFP was replaced with mRFP (-45.5 ± 9.1% to mRFP; Fig EV3A and B). No significant difference was observed either in the number of EGFP or RFP transfected neurons with (+10.5 ± 13.5% to EGFP, p = 0.70) or without Cre (+23.9 ± 20.6%, p = 0.70, one-way ANOVA, with Holm-Sidak's *post hoc*; data not illustrated).

To test the hypothesis that the Cre-dependent decrease in the number of electroporated *Kcc2*$^{lox/lox}$ neurons is due to increased apoptosis, we performed TUNEL staining and cleaved Caspase-3 (Cas3) immunostaining at E16.5 of slices from EGFP+Cre electroporated embryos. Significantly higher fractions of TUNEL^{+} and Cas3^{+} neurons were found among embryos with EGFP+Cre compared to EGFP alone (Cas3, EGFP: 0.1 ± 0.1%; EGFP+Cre: 6.7 ± 0.2%; TUNEL, EGFP: 4.3 ± 0.7%; EGFP+Cre: 15.4 ± 2%; Fig 1C and D), indicating that the decrease in neuronal number observed two days later is caused by increased apoptosis following loss of KCC2. At E16.5, no significant difference in the number of EGFP^{+} neurons was observed between the two electroporation conditions (EGFP+Cre: +2.4 ± 7.1% to EGFP, Fig 1E), suggesting that

decreased proliferation of neural progenitors is unlikely to contribute to the decrease in the number of neurons at E18.5.

To examine possible effects of KCC2 deletion on neuronal maturation, we performed whole-cell patch clamp recordings from Cre+EGFP-cotransfected (*Kcc2*$^{lox/lox(+Cre)}$) and neighboring non-transfected (*Kcc2*$^{lox/lox(-Cre)}$) pyramidal shaped-neurons in somatosensory cortical slices at postnatal day 15-17 *Kcc2*$^{lox/lox}$. In line with the efficacy of Cre-mediated ablation of KCC2 in *Kcc2*$^{lox/lox}$ animals at E18.5, net Cl^- extrusion measured under conditions of constant somatic Cl^- load [44,56] of Cre-transfected neurons was abolished, shifting E_{GABA} close to the level dictated by the Cl^- concentration of the pipette both at the soma (mean E_{GABA}, *Kcc2*$^{lox/lox(-Cre)}$: -56.4 ± 1.4 mV; *Kcc2*$^{lox/lox(+Cre)}$: -48.5 ± 0.8 mV) and at a distance of 50 µm in a dendritic location (mean E_{GABA}, *Kcc2*$^{lox/lox(-Cre)}$: -66.2 ± 1.6 mV; *Kcc2*$^{lox/lox(+Cre)}$: -51.3 ± 1.7 mV; Fig EV4A and B). However, no differences were observed (cf. [57]) in basic electrophysiological parameters, including resting membrane potential, input resistance or membrane capacitance (Fig EV4C-E), the latter used as a proxy for plasmalemmal membrane surface area and, thus, dendritic arbor complexity [26,36].

Taken together, these data indicate that cell-specific loss of KCC2 increases apoptotic cell death of late-born PNs destined for upper cortical layers, without perturbing proliferation or affecting the maturation of the above electrophysiological parameters, apart from E_{GABA}.

Ion transport-independent action of KCC2 CTD promotes the survival of migrating projection neurons

To investigate whether the ability of KCC2^{FL} to prevent the observed decrease in the number of neurons is due to the ion transport-independent role of KCC2, we examined the effects of two ion transport-dead KCC2 constructs. An N-terminally truncated KCC2 construct, which comprises the transmembrane and C-terminal domains (KCC2$^{\Delta NTD}$, Fig 2A, lower panel), or another construct, which comprises the entire CTD alone (KCC2^{CTD}, Fig 2A, lower panel) [31,34,38] were co-electroporated with Cre at E14.5 and transfected neurons were counted at E18.5 as for KCC2^{FL}. No significant difference was observed between Cre+KCC2$^{\Delta NTD}$ or Cre+KCC2^{CTD} when compared to Cre+KCC2^{FL} (Cre+KCC2$^{\Delta NTD}$: +6.0 ± 5.7% to Cre+KCC2^{FL}; Cre+KCC2^{CTD}: -12.6 ± 6.2% to Cre+KCC2^{FL}; Fig 2A and B). These data indicate that the mere CTD of KCC2 is as efficient as full-length KCC2 in preventing the loss of neurons triggered by KCC2 ablation (Fig 2B).

We next electroporated Cre+KCC2^{R952H}, a full-length disease-variant of KCC2, carrying an arginine-to-histidine substitution in its distal CTD (Fig 2A, lower panel) found in patients with seizures and neurodevelopmental disorders [38–40]. KCC2^{R952H}, upon overexpression in neocortical PNs, was previously found to confer reduced Cl^- extrusion and completely lack the ion transport-independent capacity to promote dendritic spinogenesis, indicating that this missense point mutation disrupts cytoskeletal interactions mediated by KCC2 CTD [38]. Indeed, unlike the situation with Cre+KCC2$^{\Delta NTD}$ and Cre+KCC2^{CTD}, a significant difference in the number of neurons was observed when Cre+KCC2^{R952H} was compared to Cre+KCC2^{FL} (Cre+KCC2^{R952H}: -41.6 ± 3.1% to Cre+KCC2^{FL}; Fig 2A and B).

KCC2, via molecular interactions downstream of its CTD, controls actin dynamics in dendritic spines by regulating cofilin phosphorylation [36,37], with constitutive loss of KCC2 expression resulting in cofilin hyperphosphorylation in mouse cortical neurons [36]. Cofilin, a major actin-regulating protein, has been implicated in apoptosis of cortical primary neurons [58]. To study the possible cellular mechanism downstream of KCC2 CTD action, we tested whether the apoptotic process triggered by loss of KCC2 could be prevented by compensating for cofilin hyperphosphorylation. Indeed, electroporation of Cre together with a plasmid encoding a non-phosphorylatable cofilin mutant, cofilin^{S3A} [59], was as efficient as co-electroporation of Cre+KCC2^{FL} in preventing the loss of PNs upon deletion of endogenous KCC2 expression (Cre+cofilin^{S3A}: -6.2 ± 8.9% to Cre+KCC2^{FL}; Fig 2A and B).

In sum, the above data strongly support the idea that the observed increase in apoptosis of embryonic cortical projection neurons is due to the loss of ion transport-independent actions mediated by KCC2

through its intracellular CTD. Our data strongly support the idea that the regulatory function of KCC2 in developmental apoptosis does not necessitate its plasmalemmal expression. A key observation here is that plasmids encoding transport-dead KCC2 constructs ($KCC2^{CTD}$, $KCC2^{\Delta NTD}$) were as efficient in preventing neuronal loss as full-length KCC2. N-terminal truncation of KCC2 [31,38] results in complete loss of its K-Cl cotransport activity. It has been suggested that this may interfere with its delivery to the plasma membrane [60]. However, data obtained in neurons *in vivo* demonstrate that plasmalemmal expression of KCC2 may not be necessary for ion transport-independent functions mediated by the CTD, as indeed shown in the context of spinogenesis [34]. This also appears to be the case presently, as neuronal survival following KCC2 deletion was rescued by the N-terminally truncated $KCC2^{\Delta NTD}$ as well as $KCC2^{CTD}$, the latter lacking not only the N-terminal domain but also the transmembrane domains necessary for membrane expression.

Cell death mediated by KCC2 deletion differentially affects upper cortical PNs migrating in deep *vs.* superficial layers at E18.5

Birth-dating experiments using BrdU and IUE indicate that mouse upper cortical PNs labeled at E14.5 comprise of neurons belonging to both layers II/III and IV [48,61]. Cortical PNs born at E14.5 are still migrating at E18.5 [48]. Since only a fraction of the total number of Cre-electroporated $Kcc2^{lox/lox}$ neurons underwent apoptosis, we analyzed the number of the neurons that survived by E18.5 with regard to their distribution within and outside their migratory target-region, demarcated by the upper boundary of the layer V-specific marker Ctip2. We found that the significant decrease in the number of EGFP+Cre neurons was accounted by those located below the upper boundary of layer V, *i.e.* in the lower cortical regions and below the cortical plate (EGFP+Cre: -77.1 ± 4.5% to EGFP; Fig 3A and B). No significant difference in the number of neurons that had already migrated into the upper cortical plate by E18.5 was observed (EGFP+Cre: -14.13 ± 12.5% to EGFP; Fig 3A and B). A qualitatively similar effect of Cre was observed when EGFP was replaced with mRFP, with a significantly lower number of Cre+$mRFP^{+}$ neurons below the upper boundary of the layer V-specific marker Ctip2 (mRFP+Cre: -74.4 ± 5.8% to mRFP; Fig 3C and D), but not above it (mRFP+Cre: -17.2 ± 11.8% to mRFP; Fig 3C and D). These findings suggest that among the population of progenitors targeted at E14.5, the increase in apoptosis is preferential to those yielding later migrating neurons destined for the superficial parts of the upper cortical layers II-IV [48] and thus are more likely to represent layer II/III neurons.

Interestingly, co-electroporation of Cre+$KCC2^{R952H}$ resulted in a statistically significant decrease in the number of neurons that had migrated at E18.5 to the upper cortical layers (Cre+$KCC2^{R952H}$: -33.2 ± 5.9% to Cre; Fig 3E and F). In full accordance with the inability of this mutant to promote survival (Fig 2B), no significant increase compared to the Cre-alone condition was observed in the number of Cre+$KCC2^{R952H}$ neurons that were still migrating towards the upper cortical plate (Cre+$KCC2^{R952H}$: +44.8 ± 12.5% to Cre; Fig 3E and F). In contrast, Cre+$KCC2^{FL}$ and Cre+$KCC2^{CTD}$ both showed a significantly higher number of neurons in this region (Cre+$KCC2^{FL}$: +337 ± 41.5% to Cre; Cre+$KCC2^{CTD}$: +214.4 ± 16.5% to Cre; Fig 3E and F). These findings indicate that the impact of $KCC2^{R952H}$ differs radically from that of full KCC2 deletion, affecting neurons that at E18.5 are migrating as well as those that have already reached the upper cortical layers by that time. This point mutation in the CTD has been previously shown to compromise neuronal Cl^- extrusion capacity, and it entirely abolishes the interactions of the KCC2 CTD with the actin cytoskeleton in dendritic spines [38,39]. A possible explanation of the qualitative difference in action of KCC2 deletion and this C-terminal mutation might be in their differential effect on targets downstream of the KCC2 CTD, which notably includes cofilin [36,37]. Indeed, we observed presently (see above) that neuronal loss was prevented by overexpressing a phosphorylation-resistant cofilin mutant.

Constitutive ablation of KCC2 does not alter cortical lamination but increases cell death of deep-layer migrating upper cortical layer PNs at E18.5

In light of the observed KCC2 loss-induced preferential decrease in the number of PNs still migrating at E18.5 (Fig 3A), which have not yet contributed to the cortical layers present at this stage of development, we examined whether constitutive ablation of KCC2 affects the number of neurons labeled with cortical layer-specific markers within the layers present at E18.5. To this end, we employed constitutive *Kcc2*$^{-/-}$ mouse embryos [62]. Quantitative analysis of brain sections showed that the laminar organization of the *Kcc2*$^{-/-}$ embryonic cortex at E18.5 was similar to that of their *Kcc2*$^{+/+}$ littermates, as seen by immunolabeling using cortical layer-specific markers in coronal slices from closely matched bregma regions of the developing neocortex (Fig 4). We used Cux1 to mark the late-born neurons of layers II-IV [63], Ctip2 to mark layer V neurons [64], and Tbr1 to mark early-born layer VI neurons [65] (Fig 4A-C). No difference was observed between *Kcc2*$^{+/+}$ and *Kcc2*$^{-/-}$ littermates in the thickness of the SSC layers (Cux1^{+}, *Kcc2*$^{-/-}$: -2.2 ± 2.1% to *Kcc2*$^{+/+}$; Ctip2^{+}, *Kcc2*$^{-/-}$:+2.9 ± 2.1% to *Kcc2*$^{+/+}$; Tbr1^{+} *Kcc2*$^{-/-}$: +3.4 ± 2.7% to *Kcc2*$^{+/+}$; Fig 4A-C). Our data obtained in *Kcc2*$^{lox/lox}$ mice indicate preferential increase in cell death of late-migrating upper cortical neurons but not of neurons that had reached the upper cortical plate at E18.5 (Fig 3). Consistent with this, we did not observe any significant difference in the number of neurons expressing layer-specific markers within the cortical layers formed by E18.5 between the *Kcc2*$^{+/+}$ and *Kcc2*$^{-/-}$ cortices (Cux1^{+}, *Kcc2*$^{-/-}$: -2.5 ± 2.7% to *Kcc2*$^{+/+}$; Ctip2^{+}, *Kcc2*$^{-/-}$: +1.6 ± 2.0% to *Kcc2*$^{+/+}$; Tbr1^{+} *Kcc2*$^{-/-}$: +2.1 ± 2.5% to *Kcc2*$^{+/+}$; Fig 4A-C).

We then investigated whether there is a preferential decrease in the number of upper cortical plate PNs that are still migrating at E18.5, and thus do not yet contribute to the existing cortical layers. We used IUE of EGFP at E14.5 to target upper cortical layer PN progenitors in *Kcc2*$^{-/-}$ embryos and their *Kcc2*$^{+/-}$ and *Kcc2*$^{+/+}$ littermates. No difference was observed in the total number of EGFP^{+} neurons/ROI at E18.5 between *Kcc2*$^{+/+}$ and *Kcc2*$^{+/-}$ littermates (*Kcc2*$^{+/+}$: 299.2 ± 27.6; n = 9 embryos; *Kcc2*$^{+/-}$: 307.8 ± 45.37; n = 5 embryos, p = 0.86; two-tailed t test; not illustrated) and these data were pooled. In line with the effect observed in *Kcc2*$^{lox/lox}$ embryos electroporated with EGFP+Cre (Fig 1A and B), we observed a statistically significant lower total number of EGFP^{+} neurons (*Kcc2*$^{-/-}$: -21.8 ± 7.1%; Fig 4D and E) in slices from *Kcc2*$^{-/-}$ embryos compared to the pooled data from their *Kcc2*$^{+/-}$ and *Kcc2*$^{+/+}$ littermate controls. Again, a statistically significant decrease in migrating EGFP^{+} neurons in *Kcc2*$^{-/-}$ embryos was restricted to the deep cortical regions, demarcated by the upper boundary of the Ctip2 immunosignal which labels layer V (*Kcc2*$^{-/-}$: -41.4 ± 8.3% to *Kcc2*$^{+/+}$+*Kcc2*$^{+/-}$; Fig 4F). No difference was observed in the number of migrating neurons above this zone (*Kcc2*$^{-/-}$: -7.03 ± 8.3% to *Kcc2*$^{+/+}$+*Kcc2*$^{+/-}$; Fig 4F). These data from the constitutive KCC2 knockout line consolidate our observations made in the conditional knockout indicating that loss of KCC2 does not decrease the number of cortical PNs within their target layers formed by E18.5. Moreover, they support the idea that the population of PNs affected by loss of KCC2 is delimited to neurons that are still migrating at E18.5.

In summary, we found that the loss of intracellular signaling mediated by the CTD of KCC2 in late-born upper cortical PNs increases the likelihood for their elimination during the first of two major waves of neurodevelopmental apoptosis. Our data demonstrate that the canonical role of KCC2, K-Cl cotransport [20,21], is not at play in promoting the survival of neurons during the first wave of apoptosis. This is in line with overexpression studies in embryonic and early postnatal rats suggesting kinetic inactivation of KCC2 as a Cl^{-} transporter in immature cortical projection neurons until around the time of birth [29,30,55]. Conditional deletion of KCC2 using Cre electroporation at E14.5 into *Kcc2*$^{lox/lox}$ embryos, targeting a subpopulation of late-born PNs, increased the fraction of apoptotic neurons at E16.5. Importantly, the number of neurons at E16.5 did not depend on KCC2 expression, indicating that the decrease in the number of neurons observed two days later is indeed due to enhanced cell-death and not to reduction in proliferation. Notably, our data indicate that constitutive genetic ablation of KCC2 expression does not perturb the lamination of the somatosensory cortex by E18.5, including no change in the number of neurons expressing layer-specific markers within the layers formed by this time in development. However,

we observed a selective loss of upper cortical PNs still migrating at E18.5 in both our constitutive and conditional KCC2 knockout models. Importantly, the number of neurons labeled at E14.5, which had reached the upper parts of the cortical plate at E18.5, was unaltered in both knockout models. Given that IUE at E14.5 targets progenitors that give rise to both layer IV and II/III PNs [48], it is probable that the neuronal population most susceptible to KCC2 deletion in these two mouse models belong to the upper cortical PNs that will form the superficial parts of the upper cortical plate, notably layer II/III PNs. Indeed, at the time of analysis, E18.5, the vast majority of layer II/III pyramidal neurons are still migrating in the deep parts of the cortical plate and in the IZ/SVZ [48], with little contribution yet to the nascent layer II/III. Strikingly, we found that expression of the missense KCC2 variant, $KCC2^{R952H}$, which carries a point mutation in the CTD has been found in patients with febrile seizures [38], idiopathic generalized epilepsy [39], as well as autism and schizophrenia [40], was not only unable to rescue the late-born neurons migrating at E18.5, but also decreased the number of those that had by then reached the upper cortical plate. Thus, $KCC2^{R952H}$ may present as a pathological gain-of-function mutation, with capacity to promote excessive neuroapoptosis throughout the upper cortical plate PNs. Downregulation of KCC2 has been reported in human preterm infants with white matter damage [66], suggesting that an early loss of KCC2 may be related to cerebral palsy and encephalopathy of prematurity [67]. Perturbations in neurodevelopmental apoptosis are thought to contribute to early-onset epileptic encephalopathies [68,69]. An important implication of this study is that genetic variation in *SLC12A5* or perinatal insults that result in KCC2 downregulation may promote neurodevelopmental disorders by increasing cell death during early cortical development. At a broader scale, our findings stress the importance of the pleiotropic aspects of *SLC12A5* across ontogenesis.

MATERIALS AND METHODS

Animals

The experiments were conducted according to the guidelines and with the approval of the National Animal Ethics Committee of Finland (Helsinki, Finland) and the local Animal Ethics Committee of the University of Helsinki (Helsinki, Finland). All animal procedures regarding the generation of $Kcc2^{lox/lox}$ mice followed the National Institute of Health guidelines on the use of animals (Bethesda, Maryland, USA) and were approved by the Vanderbilt University Institutional Animal Care and Use Committee (Nashville, Tennessee, USA). Both the heterozygous KCC2 mice used to generate $Kcc2^{-/-}$ (constitutive deletion model) [31,38,62] and $Kcc2^{lox/lox}$ (conditional deletion model, generated in this study) mice were housed in type II open polycarbonate cages with aspen wood bedding, within a conventional animal facility under a 12-h light-dark cycle and with food and water available *ad libitum*. The cages were enriched with wooden and cardboard play tunnels, and polycarbonate retreats. Mouse pups (P15-17) were kept together with the dams until used. E16.5-18.5 mouse embryos and P15-17 pups of either sex were used for analysis.

Generation of the $Kcc2^{lox/lox}$ line

Embryonic stem cells derived from 129/SvEvTac mice were transfected with a construct targeting the *Slc12a5* gene, encoding KCC2 protein. The construct consists of a 7.6 kb genomic DNA fragment as the long arm of recombination, followed by a loxP site, the neomycin resistance gene cassette, a second loxP site, 740 bp of genomic DNA containing exon-5, a third loxP site and a 1.1 kb short arm of recombination (Fig EV2A). Exon-5 of *Slc12a5* encodes the end of the second transmembrane domain (TM2) and a portion of the intracellular loop between TM2-TM3. Deletion of this exon results in a preterm stop codon and complete KCC2 knockout. Three hundred and sixty neomycin-resistant colonies were picked and analyzed by Southern blot. Twelve clones were identified as having successfully recombined, and two of them were injected into C57BL6 blastocysts, generating chimeric males and germline transmission. Mice carrying the allele with all three loxP sites in the *Slc12a5* gene were crossed to E2a-Cre deleter line to randomly produce

mice with a reduction from three loxP to two loxP sites. PCR genotyping identified a mouse having lost the neomycin resistance gene cassette but conserved the exon. One additional mating with E2a-Cre mice verified the functionality of the remaining two loxP sites (reduction to one loxP with loss of the exon) flanking exon-5 (Fig EV2B).

To confirm that exon-5 can be efficiently deleted after transient overexpression of Cre recombinase, we used a PCR strategy in *Kcc2*$^{lox/lox}$ cortical primary neurons. A set of primers was designed to produce a PCR product of ~180 bp in a case of successful recombination (and exon-5 deletion), and ~280 bp PCR product for the intact KCC2-flox allele. Cortical neuronal cultures were derived from E17.5 *Kcc2*$^{lox/lox}$ mouse embryos and maintained in 4-well plates in Neurobasal medium supplemented with B27 and penicillin/streptomycin mix for 8 days *in vitro* (DIV). DIV 8 cultures were transfected (0.5 µg per well) with either Cre-expression construct, or with an empty vector using Lipofectamine2000 (Thermo Fisher Scientific) according to the manufacturer's protocol. Two days later, the cultures were lysed, and genomic DNA was purified using DNA extraction kit Blood & Cell Culture DNA Mini Kit (QIAGEN). GoTaq® G2 Ready-to-Use Master Mix was used to amplify the purified genomic DNA (~100 ng) with the following primers: NB3 (forward): 5'-TTACACAAGTACTGCGGTCCATTG-3', NB4 (reverse-1): 5'-GCCTCAAGGCTATGTGTAAAGACTCA-3', NB14 (reverse-2): 5'-GACACCATCATCTGCCTCCTTCCC-3'. PCR cycling conditions were: 95 °C 2 min; 40 cycles: 95 °C 25 sec, 58 °C 25 sec, 72 °C 45 sec; 72 °C 5 min. PCR reactions were run on a 2.5% agarose gel.

In utero electroporation

In utero electroporation of timed-pregnant mice with E14.5 embryos was done as before [38], with the following modifications: timed-pregnant mice were anesthetized with isoflurane (4% induction in narcosis box, 2% during surgery at operation platform). The animals were then injected subcutaneously with the analgesic (0.1 ml, Buprenorphine, 0.05 mg/kg). A small incision was made along the abdomen, the peritoneal cavity was surgically opened, and the uterine horns were exposed. Embryos were injected intraventricularly with 1.25 µl of a solution containing Fast Green (Sigma) in sterile PBS and plasmid DNA (2-3 µg/µl). The embryos were subsequently electroporated with forceps-type electrodes (CUY650P5, Sonidel Limited) placed at 0° from the horizontal plane of the brain [49–51] with five 50 ms pulses of 45 V at 100 ms intervals delivered with a square-wave generator (CUY21vivo SC, Sonidel Limited). After the surgery, mice were injected subcutaneously with the analgesic for two days (0.15 ml, Carprofen, 5mg/kg). Mice were allowed to recover, and embryos were harvested either 48 h (E16.5) or 96 h (E18.5) post-electroporation, or at P15-17.

Expression vectors for _in utero_ electroporation

All of the plasmid constructs bearing a modified chicken β-actin promoter with a cytomegalovirus immediate early enhancer (CAG) have been described and used previously for *in utero* electroporation and transfection: Cre-recombinase (Cre; a gift from Prof. Connie Cepko, Addgene plasmid # 13775) [70], full-length KCC2 (KCC2^{FL}), N-terminally truncated KCC2 (KCC2$^{\Delta NTD}$), C-terminal domain of KCC2 (KCC2^{CTD}) [31,34], a KCC2 variant with an arginine-to-histidine substitution at position 952 of KCC2b (KCC2^{R952H}) [38], a cofilin variant with a serine-to-arginine substitution at position 3 (cofilin^{S3A}, a kind gift from Prof. Michael Frotscher) [59], and an empty expression construct (pCAGEN, a gift from Prof. Connie Cepko, Addgene plasmid # 11160) [71].

pCAG-EGFP [34,38] or pCAG-mRFP (a gift from Prof. Joseph LoTurco, Addgene plasmid #28311) [72] constructs were co-injected to fluorescently label the electroporated neurons, except in experiments with pCAG-cofilin^{S3A}-EGFP. To reduce the factor of differences in the exact postconceptional age, in part of the electroporation experiments, every second embryo within the same uterus received injection of one of two different KCC2 variant plasmid constructs, discerned by co-injection of either pCAG-EGFP or pCAG-mRFP. No differences in neuronal numbers or their distribution patterns were associated with the choice of the fluorescent reporter used (see *Results*).

For the experiments using *Kcc2*$^{lox/lox}$ animals, the total DNA concentration was kept constant at 3 µg/µl, of which the final concentration of the Cre plasmid in the mixture was 2 µg/µl, EGFP 0.3 µg/µl, and KCC2

and cofilin constructs 0.7 µg/µl. pCAGEN was added *ad* 3 µg/ml, where appropriate, to keep the total DNA concentration constant. For experiments done in *Kcc2*$^{+/+}$ and *Kcc2*$^{-/-}$ embryos, the total DNA concentration in the IUE mixture was kept at 2 µg/µl, of which the EGFP plasmid constituted 0.3 µg/µl and pCAGEN 1.7 µg/µl.

Assessment of the efficacy of KCC2-mediated Cl^- extrusion in layer 2/3 projection neurons

Acute 400-µm coronal neocortical slices were prepared from *in utero* electroporated *Kcc2*$^{lox/lox}$ mice, using methods described before [34,44]. To measure KCC2-mediated Cl^- extrusion, we used our standard whole-cell recording assay where a somatic Cl^- load (19 mM) is imposed on the neuronal soma via the recording whole-cell patch pipette [44]. Whole-cell patch-clamp recordings and confocal microscopy were performed as before [44] from EGFP-positive upper cortical layer projection neurons from slices of P15-17 mice (n = 6 animals from 4 different litters) co-electroporated *in utero* with plasmids bearing constructs encoding for EGFP and Cre. Neighboring non-transfected (EGFP-negative) neurons served as internal controls. One to four neurons per group were recorded from each slice and their averaged values used for statistical analysis. Locally applied DPNI-caged GABA (1 mM Tocris) was used to elicit photolysis-induced (375 nm UV-laser, 10 ms) $GABA_AR$-mediated currents at the soma or 50 µm away at the apical dendrite [44]. All recordings were performed in the presence of 10 µM bumetanide (Tocris), 0.5 µM TTX (Abcam), 20 µM D-AP5 (Tocris), 10 µM CNQX (Abcam) and 1 µM CGP 55845 (Abcam) in the standard extracellular solution [44,73]. Membrane potential values were corrected for series resistance effect and for a calculated liquid junction potential of 14 mV.

Tissue processing and immunohistochemistry

E18.5 mouse brains were briefly fixed by immersion in 4% PFA in PBS, cryoprotected overnight in 30% sucrose, frozen in Tissue-Tek O.C.T. Compound (Sakura FineTek), and cut into 40-µm coronal free-floating slices on a CM1900 cryostat (Leica). For cleaved-Caspase-3 staining, the E16.5 brains were cut into 16-µm coronal slices, and post-fixed with 1% PFA in PBS at room temperature prior to staining. Brain slices were washed three times for 10 min in PBS (pH 7.4) and blocked in 3% BSA, 0.3% Triton-X, and 10% goat serum in PBS for 2 hours at room temperature. Primary antibodies were incubated overnight at +4°C; sections were then washed and incubated in secondary antibodies in modified blocker solution (1% BSA, 0.3% Triton-X, 10% goat serum in PBS) for 2 hours at RT. The sections were then washed in PBS; the nuclei were stained with 4, 6-diamidino-2-phenylindole (DAPI, 2.5 µg/µl in PBS) for 10 min. The sections were mounted on glass slides with FluoroMountG (Thermo Fisher) and stored at +4°C until imaging. Antibodies used in this study were: cleaved Caspase-3 (#9661, Cell Signalling, 1:400), Cux1 (sc-13024, Santa Cruz, 1:100), Ctip2 (ab18465, Abcam, 1:250), Tbr1 (AB10554, Millipore, 1:1000), KCC2 (07-432, Millipore, 1:1000), Cre (MB3127, Millipore, 1:1000).

TUNEL labeling of apoptotic neurons

E16.5 mouse brains were briefly fixed by immersion in 4% PFA in PBS, cryoprotected overnight in 30% sucrose, frozen in Tissue-Tek O.C.T. Compound (Sakura FineTek), cut into 16-µm coronal slices on a CM1900 cryostat (Leica), mounted on positively charged glass slides (Super-FrostPlus; VWR International), and stored at −80°C. To assess the number of apoptotic neurons, we used the ApopTag Red *In Situ* Apoptosis Detection Kit (Millipore) following the manufacturer's instructions for tissue cryosections. Briefly, brain slices were post-fixed with 1% PFA in PBS at room temperature followed by treatment with Ethanol: Acetic acid (2:1) at -20°C. After fixation and washes, working strength TdT enzyme in Reaction Buffer was added to the sections and incubated at +37°C. The reaction was stopped with the Stop/Wash Buffer, and DNA fragments were stained using anti-digoxigenin Rhodamine in Blocker at room temperature. Nuclei were stained with 4, 6-diamidino-2-phenylindole (DAPI, 1 µg/µl in PBS). The sections were mounted on glass slides with FluoromountG (Thermo Fisher) and stored at +4°C until imaging.

Image acquisition and analysis

Images were collected with LSM confocal microscope equipped with LD LCI Plan-Apochromat 25x/0.8 Imm Corr objective, Axio Imager 2 light microscope equipped with ApoTome with 25x and 40x/oil immersion objectives, and Axio Imager M1 with 10x objective (all from Zeiss). Images of E16.5 brains used for TUNEL and E18.5 brains used for KCC2 IHC staining are presented as maximum intensity projections of 10 optical sections taken at 0.5 µm intervals. Representative images of E18.5 sections from *Kcc2*$^{lox/lox}$ embryos co-electroporated *in utero* at E14.5 with constructs expressing EGFP or mRFP are indicated by pseudo-color in green. All images were analyzed using FIJI [74].

Analysis of cortical layering

For the analysis of cortical lamination in E18.5 *Kcc2*$^{-/-}$ embryos and their wildtype littermates, we analyzed the cortical plate at the level of the nascent SSC at the same rostro-caudal level for each brain (approximately three mm from bregma, [75], the junction of the lateral ventricle and the caudo-putamen). The developing cortical plate was divided into three regions delineated by different layer-specific antibodies: Cux1 to mark the superficial, late-born neurons in layers II-IV [63], Ctip2 to mark the layer V neurons [64], and Tbr1 to mark layer VI neurons [65]. Cortical layer thickness and the number of neurons was assessed in a common boxed region of 600*400 µm and analyzed in FIJI [74]. After background subtraction, the layer thickness was measured perpendicular to the surface of the cortex. To quantify the number of neurons within each neocortical layer, the images of brain slices stained against Cux1, Ctip2, or Tbr1 were thresholded, and the command *Analyze particles* was used to quantify and create a mask containing ROIs of the neurons expressing the layer-specific markers. In the analysis of the total thickness of the cortical plate and the number of neurons expressing layer-specific markers within individual cortical layers, data were normalized to WT corresponding controls.

Quantification of neuronal numbers

To quantify the total number of neurons electroporated *in utero*, the number of fluorescent cells was calculated in the electroporated area in a common boxed region of 850*650 µm in a semi-automated way using FIJI [74]. The background was subtracted from the neurons expressing either EGFP or mRFP, the image was thresholded, and the command *Analyze particles* was used to create a mask containing ROIs of neurons. The neurons that were omitted by the automatic procedure were added manually. For quantification of the number of neurons that migrated to the upper cortical layers, the cortical plate was divided into upper (layers II-VI) and lower (layers V and VI, as well as the area below the cortical plate comprising both IZ and SVZ) sub regions using the Ctip2-immunostaining of layer V neurons at the same rostro-caudal level for each brain (approximately 3mm from bregma, [75]).

The percentage of the EGFP^{+} neuronal population undergoing apoptosis was quantified using activated caspase 3 (Cas-3) staining or TUNEL in slices from E16.5 *Kcc2*$^{lox/lox}$ embryos electroporated with EGFP±Cre. The background was subtracted from the Cas3^{+} neurons or TUNEL^{+} nuclei, the image was thresholded, and the command *Analyze particles* was used to create a mask containing the labeled neurons. The neurons that showed showed Cas-3 staining or DNA fragmentation were marked as apoptotic (Cas-3^{+}, TUNEL^{+}) and quantified manually.

***Slc12a5* mRNA expression**

The online source DeCoN (Developing Cortical Neuron Transcriptome Resource, http://decon.fas.harvard.edu/pyramidal/gene/Slc12a5) was used to compare expression levels of the *Slc12a5* gene (encoding KCC2) at the time points of interest (Data ref: [46]). KCC2 expression datasets were derived from isoform-deconvolution based differential RNA-sequencing of sorted cellular populations corresponding to three neuronal subclasses at specified time points during corticogenesis (E15.5, E16.5,

E18.5, and P1) [45]. Two biological replicates were used for each neuronal subtype and developmental time point (one litter of six to ten CD1 mouse embryos or pups was used as one biological replicate).

Statistics

Statistical analyses were performed in Prism 8 (GraphPad Software). Normality was tested using Kolmogorov-Smirnov test for each distribution, and significance level α was set to 5% for all tests. Normally distributed data were analyzed using one-tailed or two-tailed Student's *t*-test. For non-Gaussian distributions, the Mann-Whitney U test was used. For multiple comparisons, statistical significance was determined using one-way ANOVA with Holm-Sidak's *post-hoc* test for normally distributed data, otherwise the Kruskal-Wallis test with Dunn's *post hoc* was used. For experiments with internal control within the same slice, ANOVA with repeated measures followed by Bonferroni's *post hoc* was used. The statistical test used for each experiment is indicated in the Figure legends. Equality of group variance was estimated using the Brown-Forsythe test. No significant difference in variance was observed between the groups that were statistically compared, except for the Fig 4A, B and C panels depicting the number of neurons in cortical layers labeled with layer-specific antibodies. In this case we detected a significant difference in the variance of the analyzed groups ($p = 0.008$, Brown-Forsythe test). A non-parametric test (Kruskal-Wallis test with Dunn's *post hoc*) was used in this case. No randomization was done in this study. Due to the mechanistic and exploratory nature of this work, no statistical power analysis was used to guide sample-size estimation. Experiments on *in utero* electroporated animals were performed and analyzed in a blinded manner concerning the genetic construct used, whereas experiments on *Kcc2*$^{+/+}$ and *Kcc2*$^{-/-}$embryos were analyzed in a blinded fashion with respect to the genotype of the embryos. Based on our previous experience, for *in utero* electroporation experiments 5-13 animals from 3-5 different litters were used per experimental group. To obtain the mean number of neurons per embryo 1-3 slices were analyzed. Slices containing less than 100 electroporated neurons/ROI were excluded from statistical analysis. For electrophysiological experiments, 1-4 neurons per slice were analyzed. The sample size of each experimental group is stated in the Figure legends. Data are presented as mean ± S.E.M., except for Fig EV1 where data are presented as mean ± 95% CI.

ACKNOWLEDGMENTS

We thank Merle Kampura and Maria Partanen for excellent technical assistance and breeding of the animals, and Mari Virtanen and Alexey Pospelov for comments on the manuscript. This work was supported by grants from the Epilepsiatutkimussäätiö (to M.M.), the Finnish Academy of Science (grant SA257312 to P.U.), the Academy of Finland (grants 319237 and 294375 to K.K.), the Jane and Aatos Erkko Foundation (to KK), and the Emil Aaltonen Foundation (grants 160220 N1V and 180206 N1V to M.P.).

AUTHOR CONTRIBUTIONS

MM, PU, and MP performed the experiments and analyzed the data; ED generated the *Kcc2*$^{lox/lox}$ mouse line; MM, PU, LV, ED, KK, and MP designed the experiments; MM, KK and MP wrote the manuscript, with input from all of the coauthors.

CONFLICT OF INTEREST STATEMENT

The authors declare no conflict of interest.

REFERENCES

1. Buss RR, Sun W, Oppenheim RW (2006) Adaptive roles of programmed cell death during nervous system development. *Annu Rev Neurosci* **29**: 1–35.

2. Dekkers MPJ, Barde Y-A (2013) Developmental biology. Programmed cell death in neuronal development. *Science* **340**: 39–41.

3. Roth KA, Kuan C, Haydar TF, D'Sa-Eipper C, Shindler KS, Zheng TS, Kuida K, Flavell RA, Rakic P (2000) Epistatic and independent functions of caspase-3 and Bcl-X(L) in developmental programmed cell death. *Proc Natl Acad Sci U S A* **97**: 466–471.

4. de la Rosa EJ, de Pablo F (2000) Cell death in early neural development: beyond the neurotrophic theory. *Trends Neurosci* **23**: 454–458.

5. Blaschke AJ, Staley K, Chun J (1996) Widespread programmed cell death in proliferative and postmitotic regions of the fetal cerebral cortex. *Development* **122**: 1165–1174.

6. Rakic S, Zecevic N (2000) Programmed cell death in the developing human telencephalon. *Eur J Neurosci* **12**: 2721–2734.

7. Clancy B, Darlington R., Finlay B. (2001) Translating developmental time across mammalian species. *Neuroscience* **105**: 7–17.

8. Blanquie O, Yang J-W, Kilb W, Sharopov S, Sinning A, Luhmann HJ (2017) Electrical activity controls area-specific expression of neuronal apoptosis in the mouse developing cerebral cortex. *Elife* **6**.

9. Denaxa M, Neves G, Rabinowitz A, Kemlo S, Liodis P, Burrone J, Pachnis V (2018) Modulation of Apoptosis Controls Inhibitory Interneuron Number in the Cortex. *Cell Rep* **22**: 1710–1721.

10. Heck N, Golbs A, Riedemann T, Sun J-J, Lessmann V, Luhmann HJ (2008) Activity-Dependent Regulation of Neuronal Apoptosis in Neonatal Mouse Cerebral Cortex. *Cereb Cortex* **18**: 1335–1349.

11. Southwell DG, Paredes MF, Galvao RP, Jones DL, Froemke RC, Sebe JY, Alfaro-Cervello C, Tang Y, Garcia-Verdugo JM, Rubenstein JL, et al. (2012) Intrinsically determined cell death of developing cortical interneurons. *Nature* **491**: 109–113.

12. Verney C, Takahashi T, Bhide PG, Nowakowski RS, Caviness Jr. VS (2000) Independent Controls for Neocortical Neuron Production and Histogenetic Cell Death. *Dev Neurosci* **22**: 125–138.

13. Chowdhury TG, Jimenez JC, Bomar J, Cruz-Martin A, Cantle JP, Portera-Cailliau C (2010) Fate of Cajal-Retzius neurons in the postnatal mouse neocortex. *Front Neuroanat* **4**: 10.

14. Ledonne F, Orduz D, Mercier J, Vigier L, Grove EA, Tissir F, Angulo MC, Pierani A, Coppola E (2016) Targeted Inactivation of Bax Reveals a Subtype-Specific Mechanism of Cajal-Retzius Neuron Death in the Postnatal Cerebral Cortex. *Cell Rep* **17**: 3133–3141.

15. Achilles K, Okabe A, Ikeda M, Shimizu-Okabe C, Yamada J, Fukuda A, Luhmann HJ, Kilb W (2007) Kinetic Properties of Cl Uptake Mediated by Na+-Dependent K+-2Cl Cotransport in Immature Rat Neocortical Neurons. *J Neurosci* **27**: 8616–8627.

16. Pozas E, Paco S, Soriano E, Aguado F (2008) Cajal–Retzius cells fail to trigger the developmental expression of the Cl−extruding co-transporter KCC2. *Brain Res* **1239**: 85–91.

17. Blanquie O, Liebmann L, Hübner CA, Luhmann HJ, Sinning A (2016) NKCC1-Mediated GABAergic Signaling Promotes Postnatal Cell Death in Neocortical Cajal–Retzius Cells. *Cereb Cortex* **27**: 1644–1659.

18. Ben-Ari Y, Gaiarsa J-L, Tyzio R, Khazipov R (2007) GABA: A Pioneer Transmitter That Excites

Immature Neurons and Generates Primitive Oscillations. *Physiol Rev* **87**: 1215–1284.

19. Luhmann HJ, Fukuda A, Kilb W (2015) Control of cortical neuronal migration by glutamate and GABA. *Front Cell Neurosci* **9**: 4.

20. Rivera C, Voipio J, Payne J a, Ruusuvuori E, Lahtinen H, Lamsa K, Pirvola U, Saarma M, Kaila K (1999) The K+/Cl- co-transporter KCC2 renders GABA hyperpolarizing during neuronal maturation. *Nature* **397**: 251–255.

21. Kaila K, Price TJ, Payne JA, Puskarjov M, Voipio J (2014) Cation-chloride cotransporters in neuronal development, plasticity and disease. *Nat Rev Neurosci* **15**: 637–654.

22. Komuro H, Rakic P (1996) Intracellular Ca2+ fluctuations modulate the rate of neuronal migration. *Neuron* **17**: 275–285.

23. Owens DF, Kriegstein AR (1998) Patterns of intracellular calcium fluctuation in precursor cells of the neocortical ventricular zone. *J Neurosci* **18**: 5374–5388.

24. Allene C, Cattani A, Ackman JB, Bonifazi P, Aniksztejn L, Ben-Ari Y, Cossart R (2008) Sequential Generation of Two Distinct Synapse-Driven Network Patterns in Developing Neocortex. *J Neurosci* **28**: 12851–12863.

25. Pellegrino C, Gubkina O, Schaefer M, Becq H, Ludwig A, Mukhtarov M, Chudotvorova I, Corby S, Salyha Y, Salozhin S, et al. (2011) Knocking down of the KCC2 in rat hippocampal neurons increases intracellular chloride concentration and compromises neuronal survival. *J Physiol* **589**: 2475–2496.

26. Kelley MR, Cardarelli RA, Smalley JL, Ollerhead TA, Andrew PM, Brandon NJ, Deeb TZ, Moss SJ (2018) Locally Reducing KCC2 Activity in the Hippocampus is Sufficient to Induce Temporal Lobe Epilepsy. *EBioMedicine* **32**: 62–71.

27. Bortone D, Polleux F (2009) KCC2 Expression Promotes the Termination of Cortical Interneuron Migration in a Voltage-Sensitive Calcium-Dependent Manner. *Neuron* **62**: 53–71.

28. Spoljaric I, Spoljaric A, Mavrovic M, Seja P, Puskarjov M, Kaila K (2019) KCC2-Mediated Cl- Extrusion Modulates Spontaneous Hippocampal Network Events in Perinatal Rats and Mice. *Cell Rep* **26**: 1073-1081.

29. Inoue K, Furukawa T, Kumada T, Yamada J, Wang T, Inoue R, Fukuda A (2012) Taurine inhibits K +-Cl - cotransporter KCC2 to regulate embryonic Cl - homeostasis via with-no-lysine (WNK) protein kinase signaling pathway. *J Biol Chem* **287**: 20839–20850.

30. Friedel P, Kahle KT, Zhang J, Hertz N, Pisella LI, Buhler E, Schaller F, Duan J, Khanna AR, Bishop PN, et al. (2015) WNK1-regulated inhibitory phosphorylation of the KCC2 cotransporter maintains the depolarizing action of GABA in immature neurons. *Sci Signal* **8**: ra65–ra65.

31. Li H, Khirug S, Cai C, Ludwig A, Blaesse P, Kolikova J, Afzalov R, Coleman SK, Lauri S, Airaksinen MS, et al. (2007) KCC2 Interacts with the Dendritic Cytoskeleton to Promote Spine Development. *Neuron* **56**: 1019–1033.

32. Horn Z, Ringstedt T, Blaesse P, Kaila K, Herlenius E (2010) Premature expression of KCC2 in embryonic mice perturbs neural development by an ion transport-independent mechanism. *Eur J Neurosci* **31**: 2142–2155.

33. Gauvain G, Chamma I, Chevy Q, Cabezas C, Irinopoulou T, Bodrug N, Carnaud M, Levi S, Poncer JC (2011) The neuronal K-Cl cotransporter KCC2 influences postsynaptic AMPA receptor content and lateral diffusion in dendritic spines. *Proc Natl Acad Sci* **108**: 15474–15479.

34. Fiumelli H, Briner A, Puskarjov M, Blaesse P, Belem BJ, Dayer AG, Kaila K, Martin J-L, Vutskits L (2013)

An Ion Transport-Independent Role for the Cation-Chloride Cotransporter KCC2 in Dendritic Spinogenesis In Vivo. *Cereb Cortex* **23**: 378–388.

35. Awad PN, Amegandjin CA, Szczurkowska J, Carriço JN, Fernandes do Nascimento AS, Baho E, Chattopadhyaya B, Cancedda L, Carmant L, Di Cristo G (2018) KCC2 Regulates Dendritic Spine Formation in a Brain-Region Specific and BDNF Dependent Manner. *Cereb Cortex* **28**: 4049–4062.

36. Llano O, Smirnov S, Soni S, Golubtsov A, Guillemin I, Hotulainen P, Medina I, Nothwang HG, Rivera C, Ludwig A (2015) KCC2 regulates actin dynamics in dendritic spines via interaction with β-PIX. *J Cell Biol* **209**: 671–686.

37. Chevy Q, Heubl M, Goutierre M, Backer S, Moutkine I, Eugène E, Bloch-Gallego E, Lévi S, Poncer JC (2015) KCC2 Gates Activity-Driven AMPA Receptor Traffic through Cofilin Phosphorylation. *J Neurosci* **35**: 15772–15786.

38. Puskarjov M, Seja P, Heron SE, Williams TC, Ahmad F, Iona X, Oliver KL, Grinton BE, Vutskits L, Scheffer IE, et al. (2014) A variant of KCC2 from patients with febrile seizures impairs neuronal Cl- extrusion and dendritic spine formation. *EMBO Rep* **15**: 723–729.

39. Kahle KT, Merner ND, Friedel P, Silayeva L, Liang B, Khanna A, Shang Y, Lachance-Touchette P, Bourassa C, Levert A, et al. (2014) Genetically encoded impairment of neuronal KCC2 cotransporter function in human idiopathic generalized epilepsy. *EMBO Rep* **15**: 766–774.

40. Merner ND, Chandler MR, Bourassa C, Liang B, Khanna AR, Dion P, Rouleau GA, Kahle KT (2015) Regulatory domain or CpG site variation in SLC12A5, encoding the chloride transporter KCC2, in human autism and schizophrenia. *Front Cell Neurosci* **9**: 386.

41. Wang C, Shimizu-Okabe C, Watanabe K, Okabe A, Matsuzaki H, Ogawa T, Mori N, Fukuda A, Sato K (2002) Developmental changes in KCC1, KCC2, and NKCC1 mRNA expressions in the rat brain. *Dev Brain Res* **139**: 59–66.

42. Uvarov P, Ludwig A, Markkanen M, Pruunsild P, Kaila K, Delpire E, Timmusk T, Rivera C, Airaksinen MS (2007) A novel N-terminal isoform of the neuron-specific K-Cl cotransporter KCC2. *J Biol Chem* **282**: 30570–30576.

43. Uvarov P, Ludwig A, Markkanen M, Soni S, Hübner CA, Rivera C, Airaksinen MS (2009) Coexpression and heteromerization of two neuronal K-Cl cotransporter isoforms in neonatal brain. *J Biol Chem* **284**: 13696–13704.

44. Puskarjov M, Fiumelli H, Briner A, Bodogan T, Demeter K, Lacoh C-M, Mavrovic M, Blaesse P, Kaila K, Vutskits L (2017) K-Cl Cotransporter 2-mediated Cl- Extrusion Determines Developmental Stage-dependent Impact of Propofol Anesthesia on Dendritic Spines. *Anesthesiology* **126**: 855–867.

45. Molyneaux BJ, Goff LA, Brettler AC, Chen H-H, Brown JR, Hrvatin S, Rinn JL, Arlotta P (2015) DeCoN: Genome-wide Analysis of In Vivo Transcriptional Dynamics during Pyramidal Neuron Fate Selection in Neocortex. *Neuron* **85**: 275–288.

46. Molyneaux BJ, Goff LA, Brettler AC, Chen H-H, Brown JR, Hrvatin S, Rinn JL, Arlotta P (2015) DeCoN: The Developing Cortical Neuron Transcriptome Resource (http://decon.fas.harvard.edu/pyramidal/gene/Slc12a5) [DATASET]

47. Stein V, Hermans-Borgmeyer I, Jentsch TJ, Hübner CA (2004) Expression of the KCl cotransporter KCC2 parallels neuronal maturation and the emergence of low intracellular chloride. *J Comp Neurol* **468**: 57–64.

48. Langevin LM, Mattar P, Scardigli R, Roussigné M, Logan C, Blader P, Schuurmans C (2007) Validating in utero electroporation for the rapid analysis of gene regulatory elements in the murine

telencephalon. *Dev Dyn* **236**: 1273–1286.

49. Borrell V, Yoshimura Y, Callaway EM (2005) Targeted gene delivery to telencephalic inhibitory neurons by directional in utero electroporation. *J Neurosci Methods* **143**: 151–158.

50. Niwa M, Kamiya A, Murai R, Kubo K, Gruber AJ, Tomita K, Lu L, Tomisato S, Jaaro-Peled H, Seshadri S, et al. (2010) Knockdown of DISC1 by In Utero Gene Transfer Disturbs Postnatal Dopaminergic Maturation in the Frontal Cortex and Leads to Adult Behavioral Deficits. *Neuron* **65**: 480–489.

51. Quiquempoix M, Fayad SL, Boutourlinsky K, Leresche N, Lambert RC, Bessaih T (2018) Layer 2/3 Pyramidal Neurons Control the Gain of Cortical Output. *Cell Rep* **24**: 2799-2807.

52. Khalilov I, Chazal G, Chudotvorova I, Pellegrino C, Corby S, Ferrand N, Gubkina O, Nardou R, Tyzio R, Yamamoto S, et al. (2011) Enhanced synaptic activity and epileptiform events in the embryonic KCC2 deficient hippocampus. *Front Cell Neurosci* **5**: 23.

53. Gulyás AI, Sík A, Payne JA, Kaila K, Freund TF (2001) The KCl cotransporter, KCC2, is highly expressed in the vicinity of excitatory synapses in the rat hippocampus. *Eur J Neurosci* **13**: 2205–2217.

54. Kovács K, Basu K, Rouiller I, Sík A (2014) Regional differences in the expression of K+–Cl− 2 cotransporter in the developing rat cortex. *Brain Struct Funct* **219**: 527–538.

55. Cancedda L, Fiumelli H, Chen K, Poo MM (2007) Excitatory GABA action is essential for morphological maturation of cortical neurons in vivo. *J Neurosci* **27**: 5224–5235.

56. Khirug S, Huttu K, Ludwig A, Smirnov S, Voipio J, Rivera C, Kaila K, Khiroug L (2005) Distinct properties of functional KCC2 expression in immature mouse hippocampal neurons in culture and in acute slices. *Eur J Neurosci* **21**: 899–904.

57. Goutierre M, Al Awabdh S, Donneger F, François E, Gomez-Dominguez D, Irinopoulou T, Menendez de la Prida L, Poncer JC (2019) KCC2 Regulates Neuronal Excitability and Hippocampal Activity via Interaction with Task-3 Channels. *Cell Rep* **28**: 91-103.

58. Liu T, Wang F, LePochat P, Woo J-AA, Bukhari MZ, Hong KW, Trotter C, Kang DE (2017) Cofilin-mediated Neuronal Apoptosis via p53 Translocation and PLD1 Regulation. *Sci Rep* **7**: 11532.

59. Chai X, Zhao S, Fan L, Zhang W, Lu X, Shao H, Wang S, Song L, Failla A V., Zobiak B, et al. (2016) Reelin and cofilin cooperate during the migration of cortical neurons: A quantitative morphological analysis. *Development* **1**: 1029–1040.

60. Friedel P, Ludwig A, Pellegrino C, Agez M, Jawhari A, Rivera C, Medina I (2017) A Novel View on the Role of Intracellular Tails in Surface Delivery of the Potassium-Chloride Cotransporter KCC2. *eNeuro* **4**.

61. Ferrere A, Vitalis T, Gingras H, Gaspar P, Cases O (2006) Expression of Cux-1 and Cux-2 in the developing somatosensory cortex of normal and barrel-defective mice. *Anat Rec A Discov Mol Cell Evol Biol* **288**: 158–165.

62. Vilen H, Eerikäinen S, Tornberg J, Airaksinen MS, Savilahti H (2001) Construction of gene-targeting vectors: a rapid Mu in vitro DNA transposition-based strategy generating null, potentially hypomorphic, and conditional alleles. *Transgenic Res* **10**: 69–80.

63. Nieto M, Monuki ES, Tang H, Imitola J, Haubst N, Khoury SJ, Cunningham J, Gotz M, Walsh CA (2004) Expression of Cux-1 and Cux-2 in the subventricular zone and upper layers II-IV of the cerebral cortex. *J Comp Neurol* **479**: 168–180.

64. Hand R, Polleux F (2011) Neurogenin2 regulates the initial axon guidance of cortical pyramidal neurons projecting medially to the corpus callosum. *Neural Dev* **6**: 30.

65. Hevner RF, Shi L, Justice N, Hsueh Y-P, Sheng M, Smiga S, Bulfone A, Goffinet AM, Campagnoni AT, Rubenstein JL. (2001) Tbr1 Regulates Differentiation of the Preplate and Layer 6. *Neuron* **29**: 353–366.

66. Robinson S, Mikolaenko I, Thompson I, Cohen ML, Goyal M (2010) Loss of Cation-Chloride Cotransporter Expression in Preterm Infants With White Matter Lesions: Implications for the Pathogenesis of Epilepsy. *J Neuropathol Exp Neurol* **69**: 565–572.

67. Coq J-O, Delcour M, Ogawa Y, Peyronnet J, Castets F, Turle-Lorenzo N, Montel V, Bodineau L, Cardot P, Brocard C, et al. (2018) Mild Intrauterine Hypoperfusion Leads to Lumbar and Cortical Hyperexcitability, Spasticity, and Muscle Dysfunctions in Rats: Implications for Prematurity. *Front Neurol* **9**: 423.

68. Beal JC, Cherian K, Moshe SL (2012) Early-onset epileptic encephalopathies: Ohtahara syndrome and early myoclonic encephalopathy. *Pediatr Neurol* **47**: 317–323.

69. Saitsu H, Yamashita S, Tanaka Y, Tsurusaki Y, Nakashima M, Miyake N, Matsumoto N (2014) Compound heterozygous BRAT1 mutations cause familial Ohtahara syndrome with hypertonia and microcephaly. *J Hum Genet* **59**: 687–690.

70. Matsuda T, Cepko CL (2007) Controlled expression of transgenes introduced by in vivo electroporation. *Proc Natl Acad Sci U S A* **104**: 1027–1032.

71. Matsuda T, Cepko CL (2004) Electroporation and RNA interference in the rodent retina in vivo and in vitro. *Proc Natl Acad Sci* **101**: 16–22.

72. Manent J-B, Wang Y, Chang Y, Paramasivam M, LoTurco JJ (2009) Dcx reexpression reduces subcortical band heterotopia and seizure threshold in an animal model of neuronal migration disorder. *Nat Med* **15**: 84–90.

73. Puskarjov M, Ahmad F, Khirug S, Sivakumaran S, Kaila K, Blaesse P (2015) BDNF is required for seizure-induced but not developmental up-regulation of KCC2 in the neonatal hippocampus. *Neuropharmacology* **88**:.

74. Schindelin J, Arganda-Carreras I, Frise E, Kaynig V, Longair M, Pietzsch T, Preibisch S, Rueden C, Saalfeld S, Schmid B, et al. (2012) Fiji: an open-source platform for biological-image analysis. *Nat Methods* **9**: 676–682.

75. Paxinos G (2007) *Atlas of the developing mouse brain : at E17.5, PO, and P6*. Academic Press.

FIG CAPTIONS

Fig 1. Genetic loss of KCC2 promotes apoptosis of embryonic neocortical projection neurons *in vivo*

A Representative images of E18.5 coronal cortical sections from *Kcc2*$^{lox/lox}$ embryos electroporated *in utero* at E14.5 with plasmids encoding EGFP, EGFP+Cre (Cre) or EGFP+Cre+KCC2^{FL} (Cre+KCC2^{FL}). DAPI staining (blue) marks cell nuclei. UCP, upper cortical plate; LCP, lower cortical plate; Sp, subplate; IZ, intermediate zone. Scale bar: 50 μm.

B Quantification of the number of EGFP^{+} neurons/ROI from embryos electroporated with constructs in (A). Statistical significance was determined using one-way ANOVA with Holm-Sidak's *post hoc* test, $^{**}P < 0.01$. Data are presented as mean ± S.E.M., n (EGFP) = 8 embryos; n (Cre) = 8 embryos; n (Cre+KCC2^{FL}) = 13 embryos.

C Representative image of cleaved Caspase 3 (Cas-3, upper panel) and TUNEL (lower panel) staining in coronal sections from *Kcc2*$^{lox/lox}$ cortex at E16.5 electroporated with EGFP or EGFP+Cre are shown. Arrowheads point to neurons expressing Cas-3 (upper panel) and TUNEL (lower panel). DAPI staining (blue) marks cell nuclei. CP, cortical plate; VZ, ventricular zone; SVZ, subventricular zone; Sp, subplate; IZ, intermediate zone. Large scale bar: 50 μm, small scale bar: 20 μm.

D Quantification of the percentage of EGFP^{+} neurons expressing apoptotic markers at E16.5 from embryos electroporated with EGFP ± Cre. Statistical significance was determined using Mann-Whitney U test (Cas-3); and two-tailed *t* test (TUNEL), $^{***}P < 0.001$. Data are presented as mean ± S.E.M., n (-Cre) = 6 embryos; n (+Cre) = 6 embryos.

E The number of EGFP+Cre neurons as a percentage of neurons expressing EGFP alone. Statistical significance was determined using a two-tailed Student's *t* test. Data are presented as mean ± S.E.M., n = 6 embryos.

Fig 2. Ion transport-independent actions of KCC2 CTD promote the survival of migrating projection neurons

A Top: Representative images of E18.5 coronal cortical brain sections from *Kcc2*$^{lox/lox}$ embryos electroporated *in utero* at E14.5 together with plasmid constructs encoding Cre, a fluorescent marker (EGFP or mRFP, both pseudo-colored in green) and one of the following constructs: KCC2$^{\Delta NTD}$, KCC2^{CTD}, KCC2^{R952H}, or cofilin^{S3A}. DAPI staining (blue) marks cell nuclei. UCP, upper cortical plate; LCP, lower cortical plate; Sp, subplate; IZ, intermediate zone. Scale bar: 50 μm. Bottom: schematic representation of the KCC2 constructs.

B Quantification of the number of transfected neurons/ROI from embryos electroporated with constructs in (A). The mean number of transfected neurons from embryos electroporated with Cre+KCC2^{FL} taken from Fig 1B shown as dotted line. Statistical significance was determined using one-way ANOVA with Holm-Sidak's *post hoc* test, $^{**}P < 0.01$ to Cre+KCC2^{FL}. Data are presented as mean ± S.E.M., n (KCC2$^{\Delta NTD}$) = 7 embryos; n (Cre+KCC2^{CTD}) = 9 embryos; n (Cre+KCC2^{R952H}) = 9 embryos; n (Cre+cofilin^{S3A}) = 8 embryos.

Fig 3. Cell death mediated by KCC2 deletion differentially affects upper cortical PNs migrating in deep- *vs.* superficial-layers at E18.5

A Representative image of E18.5 coronal cortical sections stained for layer V marker Ctip2 (red) from *Kcc2*$^{lox/lox}$ embryos electroporated *in utero* at E14.5 with plasmid constructs encoding EGFP or EGFP+Cre

(Cre). Upper boundary of layer V indicted with dotted line. EGFP signal is shown as green pseudocolor. DAPI staining (blue) marks cell nuclei. Sp, subplate; IZ, intermediate zone. Scale bar = 50 µm.

B Number of EGFP+Cre neurons migrating above (II-IV) and below (V-VI/IZ-SVZ) the upper border of layer V normalized to respective data from embryos electroporated with EGFP alone. Statistical significance was determined using one-way ANOVA with Holm-Sidak's *post hoc* test, ***P < 0.001 to EGFP. Data are presented as mean ± S.E.M., n (EGFP+Cre) = 8 embryos; n (EGFP) = 8 embryos.

C Representative image of E18.5 coronal brain sections stained for layer V marker Ctip2 (red) from *Kcc2*$^{lox/lox}$ embryos electroporated *in utero* at E14.5 with plasmid constructs encoding mRFP or mRFP+Cre (Cre). Upper boundary of layer V indicted with dotted line. Sp, subplate; IZ, intermediate zone. Scale bar = 50 µm. mRFP signal is shown as green pseudocolor. DAPI staining (blue) marks cell nuclei.

D Number of mRFP+Cre neurons migrating above (II-IV) and below (V-VI/IZ-SVZ) the upper border of layer V normalized to respective data from embryos electroporated with mRFP alone. Statistical significance was determined using one-way ANOVA with Holm-Sidak's *post hoc* test, ***P < 0.001 to mRFP. Data are presented as mean ± S.E.M., n (mRFP+Cre) = 5 embryos; n (mRFP) = 5 embryos.

E Representative image of E18.5 coronal cortical sections stained for layer V marker Ctip2 (red) from *Kcc2*$^{lox/lox}$ embryos co-electroporated *in utero* at E14.5 with plasmids encoding a fluorescent marker (green) together and Cre+KCC2^{FL}, Cre+KCC2^{CTD}, or Cre+KCC2^{R952H}. DAPI staining (blue) marks cell nuclei. Upper boundary of layer V indicted with dotted line. Sp, subplate; IZ, intermediate zone. Scale bar = 50 µm.

F Number of transfected neurons migrating above (II-IV, left) and below (V-VI/IZ-SVZ, right) the upper border of layer V in embryos electroporated with constructs in (E) normalized to respective data from embryos electroporated with Cre. Statistical significance was determined using one-way ANOVA with Holm-Sidak's *post hoc* test, *P < 0.05, **P < 0.01, ***P < 0.001 to Cre. Data are presented as mean ± S.E.M., n (Cre+KCC2^{FL}) = 13 embryos; n (Cre+KCC2^{CTD}) = 9 embryos; n (Cre+KCC2^{R952H}) = 9 embryos.

Fig 4. Constitutive ablation of KCC2 does not alter cortical lamination but increases cell death of deep-layer migrating upper cortical layer PNs at E18.5

A, B, C The layer thickness and neuronal number within each layer was assessed using layer-specific markers in *Kcc2*$^{-/-}$and *Kcc2*$^{+/+}$ embryos at E18.5. Cux1 was used to label layers II-IV (A), Ctip2 to label layer V (B), and Tbr1 to label layer VI (C). Dashed white lines in the representative images in (A-C) indicate upper and lower layer boundaries. Sp, subplate. Statistical significance was determined using Kruskal-Wallis test with Dunn's *post hoc* (neuronal numbers) and one-way ANOVA with Holm-Sidak's *post hoc* (layer thickness). Data are presented as mean ± S.E.M., n = 11 embryos for both genotypes. Scale bar = 50 µm.

D Representative image of E18.5 coronal cortical sections stained for layer V marker Ctip2 (red) in *Kcc2*$^{-/-}$ and *Kcc2*$^{+/+}$ embryos electroporated *in utero* at E14.5 with a plasmid encoding EGFP (green). DAPI staining (blue) marks cell nuclei. Upper boundary of layer V indicted with dotted line. Sp, subplate; IZ, intermediate zone. Scale bar = 50 µm.

E Neurons from the brain sections in (D) were quantified and the total number of EGFP^{+} neurons in the *Kcc2*$^{-/-}$ sections is presented as a percentage of pooled *Kcc2*$^{+/+}$ and *Kcc2*$^{+/-}$ values. Statistical significance was determined using one-tailed Student's *t* test, *P < 0.05. Data are presented as mean ± S.E.M., n (*Kcc2*$^{+/+}$ + *Kcc2*$^{+/-}$) = 14 embryos; n (Kcc2$^{-/-}$) = 9 embryos.

F Number of EGFP$^+$ neurons in *Kcc2*$^{-/-}$ embryos migrating above (II-IV) and below (V-VI/IZ-SVZ) the upper border of layer V normalized to respective pooled data from *Kcc2*$^{+/+}$ and *Kcc2*$^{+/-}$ embryos. Statistical significance was determined using one-way ANOVA with Holm-Sidak's *post hoc* test, $^{**}P < 0.01$ to *Kcc2*$^{+/+}$ + *Kcc2*$^{+/-}$. Data are presented as mean ± S.E.M., n (*Kcc2*$^{+/+}$ + *Kcc2*$^{+/-}$) = 14 embryos; n (Kcc2$^{-/-}$) = 9 embryos.

Fig EV1. KCC2 mRNA expression in embryonic mouse cortical projection neurons

Developmental expression of the mRNA transcripts encoding KCC2 (*Slc12a5*) measured by RNAseq in the embryonic mouse neocortical projection neurons at E15.5, E16.5, E18.5 and P1 in the purified callosal projection neurons (CPN), subcortical projection neurons (ScPN), and corticothalamic/subplate neurons (CthPN) (http://decon.fas.harvard.edu/pyramidal/gene/Slc12a5). Data are presented as mean ± 95% CI. n (biological replicates) = 2 mouse litters/age point; n (technical replicates) = 6-10 animals/litter. FPKM, Fragments Per Kilobase of transcript per Million mapped reads. Dotted line indicates detectable expression level (FPKM ≥ 2; [37]).

Fig EV2. Cre-lox strategy to delete *Kcc2 in vitro* and *in vivo*

A Schematic representation of the wild-type *Kcc2* allele (exons 2 to 7) and a targeting vector used to generate *Kcc2*$^{lox/lox}$ mouse line. Exons are depicted as yellow rectangles and loxP sites as red triangles. A neomycin cassette surrounded by two loxP sites inserted into intron 4. A thymidine kinase cassette (TK) was used as a negative selection marker. The thymidine kinase and neomycin cassettes both were expressed under the control of the phosphoglycerate kinase (PGK) promoter.

B Functionality of the loxP sites in the *Kcc2*$^{lox/lox}$ mice was verified by crossing these mice with E2a-CRE deleter mice. PCR analysis revealed only one amplicon, which corresponds to the recombinant allele.

C *Kcc2* allele can be rapidly inactivated by transient (48 hours) overexpression of Cre-recombinase in dissociated neuronal cultures plated from *Kcc2*$^{lox/lox}$ embryos. PCR detects ~180 bp recombinant amplicon corresponding to the inactivated *Kcc2* allele in the cultures transfected with the Cre-recombinase (+Cre), but not in the control (-Cre) cultures. Since the standard Lipofectamin2000 transfection protocol results in less than 1% of transfected neurons in dissociated neuronal cultures, PCR product ~300 bp corresponding to the intact *Kcc2* allele in non-transfected neurons is also present on the agarose gel.

D Representative images of E18.5 coronal brain sections prepared from *Kcc2*$^{lox/lox}$ embryos co-electroporated *in utero* at E14.5 with constructs encoding EGFP (green, upper panel) and Cre-recombinase together with EGFP (lower panel) and subsequently analyzed at 18.5 by IHC with anti-KCC2 antibody (red). DAPI staining (blue) marks cell nuclei. Arrowheads point to neurons expressing EGFP. UCP, upper cortical plate; LCP, lower cortical plate; Sp, subplate; IZ, intermediate zone. Scale bar = 50 µm.

E Quantification of the number of KCC2$^+$ neurons as a percentage of EGFP$^+$ neurons from embryos electroporated with EGFP alone (-Cre) or with EGFP+Cre (+Cre). Statistical significance was determined using Mann-Whitney U test, $^{***}P < 0.001$. Data are presented as mean ± S.E.M., n (-Cre) = 14 embryos; n (+Cre) = 8 embryos.

F Representative images of E18.5 coronal brain sections prepared from *Kcc2*$^{lox/lox}$ embryos, co-electroporated *in utero* at E14.5 with Cre-recombinase and EGFP (green) expression constructs, and subsequently analyzed by IHC with anti-Cre antibody (red) at E18.5. DAPI staining (blue) marks cell nuclei. Arrowheads point to neurons expressing EGFP. UCP, upper cortical plate; LCP, lower cortical plate; Sp, subplate; Scale bar = 50 µm.

G Quantification of Cre^+ neurons as a percentage of $EGFP^+$ neurons in E18.5 coronal brain sections of *Kcc2*$^{lox/lox}$ embryos (n = 11) co-electroporated *in utero* at E14.5 with Cre-recombinase and EGFP expression constructs. Data are presented as mean ± S.E.M.

Fig EV3. In utero co-electroporation of mRFP and Cre results in loss of embryonic neocortical PNs *in vivo*

A Representative images of E18.5 coronal cortical sections from *Kcc2*$^{lox/lox}$ embryos electroporated *in utero* at E14.5 with plasmids encoding mRFP or mRFP+Cre (Cre). DAPI staining (blue) marks cell nuclei. UCP, upper cortical plate; LCP, lower cortical plate; Sp, subplate; IZ, intermediate zone. Scale bar: 50 µm.

B Quantification of the number of $mRFP^+$ neurons/ROI from embryos electroporated with constructs in (A). Statistical significance was determined using two-tailed Student's *t*-test, $*P < 0.05$. Data are presented as mean ± S.E.M., n (mRFP) = 5 embryos; n (Cre) = 5 embryos.

Fig EV4: Abolished Cl^- extrusion capacity of upper cortical PNs following conditional deletion of KCC2 in *Kcc2*$^{lox/lox}$ mice

A Sample recordings of GABA uncaging–induced currents (I_{GABA}) in neighboring postnatal day (P) 15-17 projection neurons EGFP-positive Cre-transfected (*Kcc2*$^{lox/lox(+Cre)}$) and GFP-negative non-transfected (*Kcc2*$^{lox/lox(-Cre)}$) neurons at the soma (bottom traces, black circles) and at a distance 50 µm away from soma along the apical dendrite (top traces, grey circles). Horizontal bar indicates a 10-ms uncaging flash of UV light.

B Mean somatic and apical dendritic E_{GABA} values in neighboring EGFP-positive Cre-transfected (*Kcc2*$^{lox/lox(+Cre)}$) and EGFP-negative non-transfected (*Kcc2*$^{lox/lox(-Cre)}$) neurons. [GHK]: theoretical E_{GABA} level denoted by the dotted line predicted by the Goldman-Hodgkin-Katz voltage equation under the present experimental conditions in the absence of active anion regulation. Statistical significance was determined using repeated measures one-way ANOVA with Bonferroni's *post hoc* test, $**P < 0.01$, $***P < 0.001$. Data are presented as mean ± S.E.M., n = 10 slices from 6 embryos, 1-4 neurons recorded per group in each slice.

C, D, E Resting membrane potential (V_m) (C), input resistance (R_{in}) (D) and membrane capacitance (C_m) (E) from neurons recorded in (B). Statistical significance was determined using paired two-tailed Student's *t* test. Data are presented as mean ± S.E.M., n = 10 slices from 6 embryos, 1-4 neurons recorded per group in each slice.

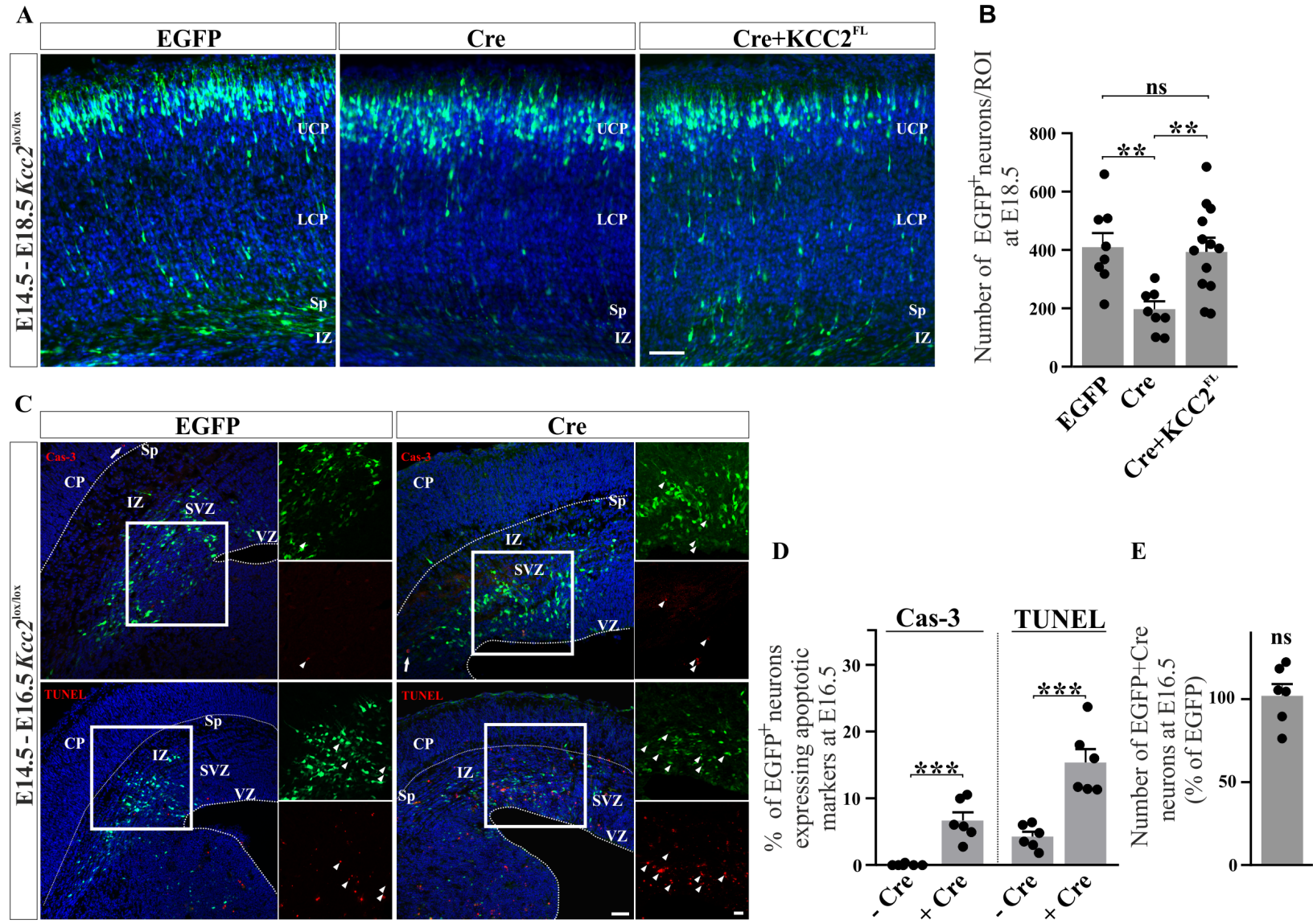
A
EGFP
Cre
Cre+KCC2FL
E14.5 - E18.5 Kcc2lox/lox
UCP
LCP
Sp
IZ
B
Number of EGFP+neurons/ROI at E18.5
ns
**
**
800
600
400
200
0
EGFP
Cre
Cre+KCC2FL
C
EGFP
Cre
E14.5 - E16.5 Kcc2lox/lox
Cas-3
TUNEL
CP
IZ
SVZ
VZ
Sp
D
Cas-3
TUNEL
% of EGFP+neurons expressing apoptotic markers at E16.5
***
***
30
20
10
0
- Cre
+ Cre
- Cre
+ Cre
E
Number of EGFP+Cre neurons at E16.5 (% of EGFP)
ns
100
50
0

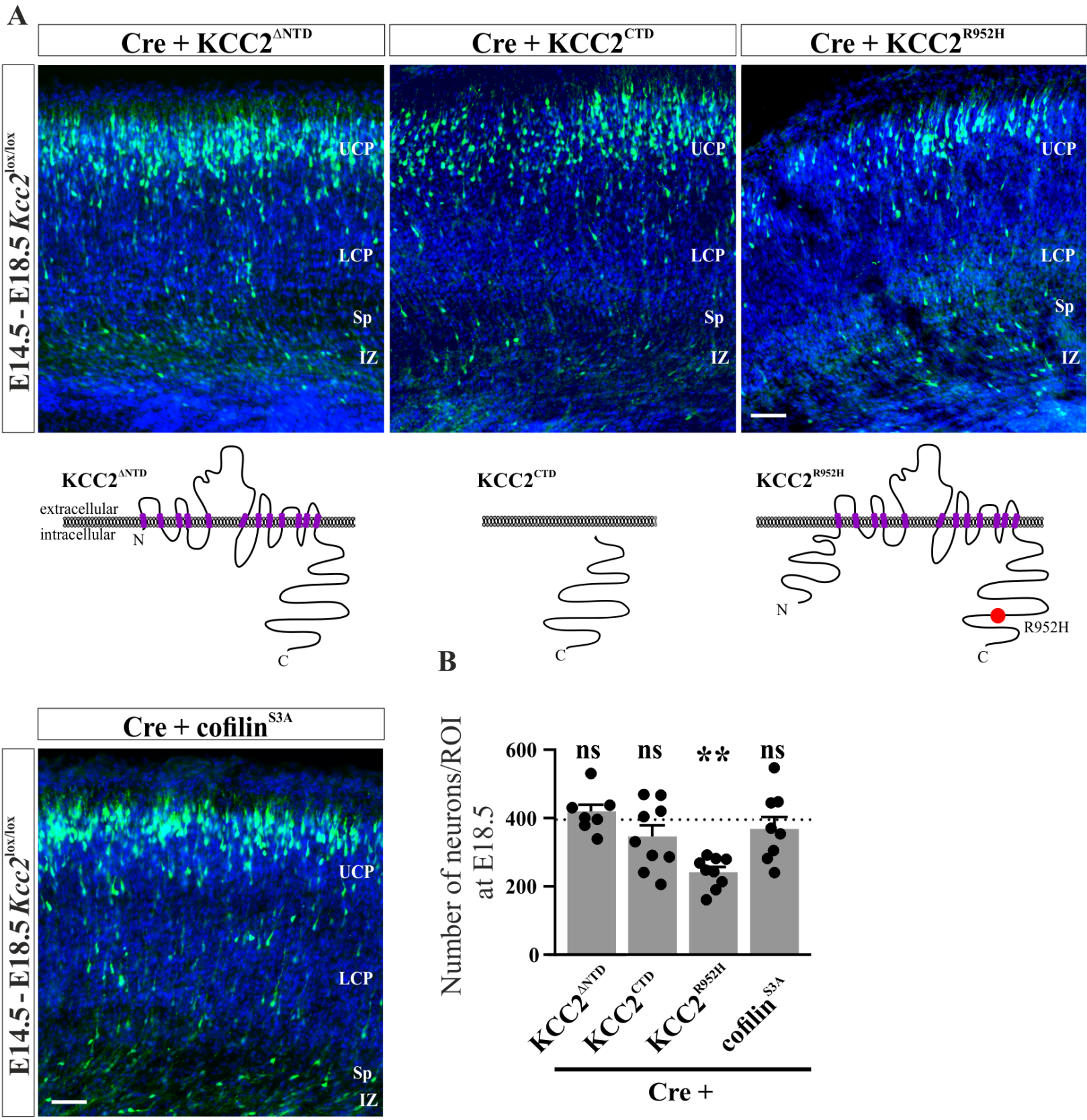
A
Cre + KCC2ΔNTD
Cre + KCC2CTD
Cre + KCC2R952H
E14.5 - E18.5 Kcc2lox/lox
UCP
LCP
Sp
IZ
KCC2ΔNTD
extracellular
intracellular
N
C
KCC2CTD
KCC2R952H
R952H
B
Cre + cofilinS3A
Number of neurons/ROI at E18.5
600
400
200
0
ns
ns
**
ns
KCC2ΔNTD
KCC2CTD
KCC2R952H
cofilinS3A
Cre +

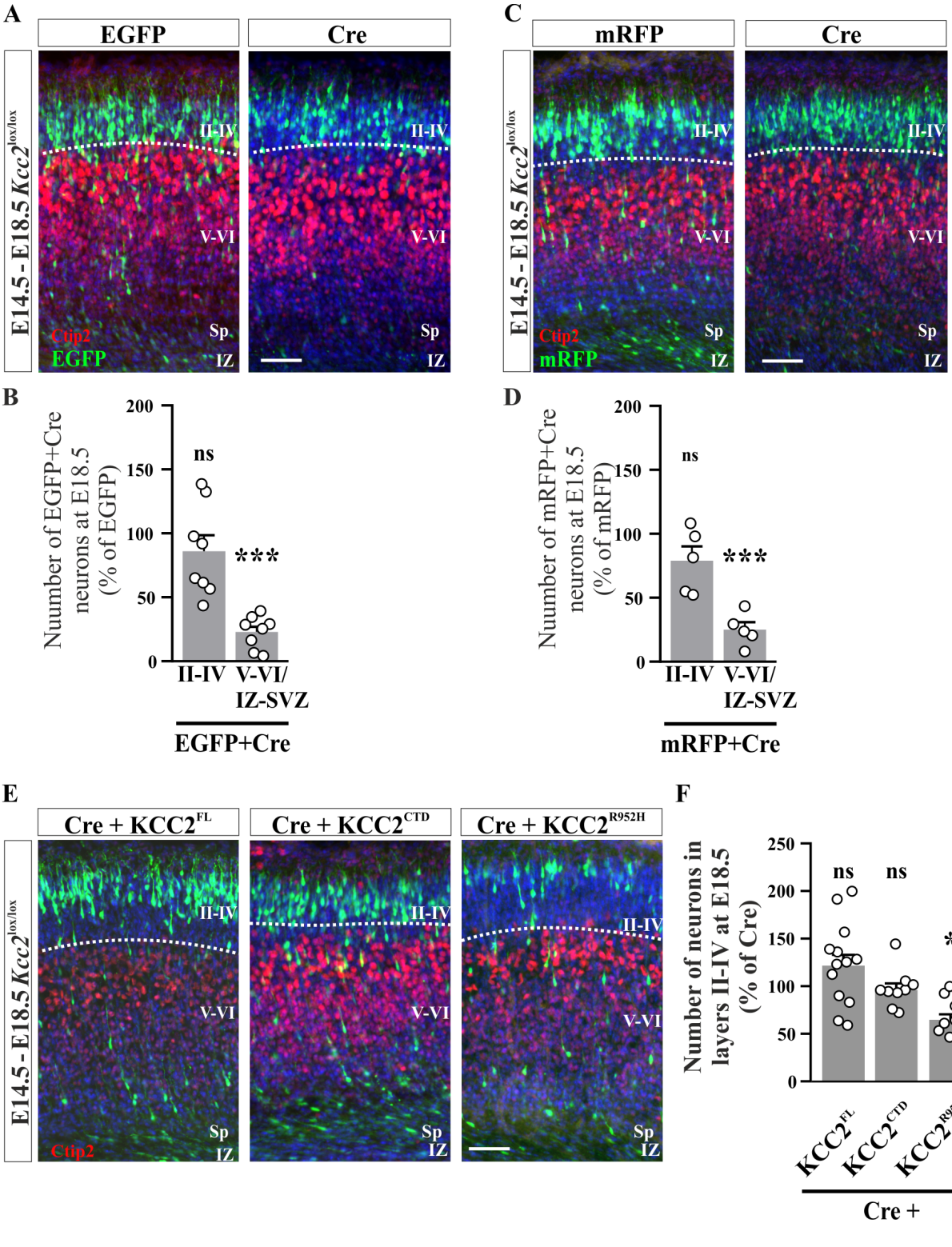
A
EGFP
Cre
E14.5 - E18.5 Kcc2lox/lox
II-IV
V-VI
Ctip2
EGFP
Sp
IZ
C
mRFP
Cre
mRFP
B
Nuumber of EGFP+Cre neurons at E18.5 (% of EGFP)
200
150
100
50
0
ns
***
II-IV
V-VI/ IZ-SVZ
EGFP+Cre
D
Nuumber of mRFP+Cre neurons at E18.5 (% of mRFP)
mRFP+Cre
E
Cre + KCC2FL
Cre + KCC2CTD
Cre + KCC2R952H
F
Number of neurons in layers II-IV at E18.5 (% of Cre)
250
200
150
100
50
0
ns
ns
*
KCC2FL
KCC2CTD
KCC2R952H
Cre +
Number of neurons in layers V-VI /IZ-SVZ at E18.5 (% of Cre)
800
600
400
200
***
**
ns

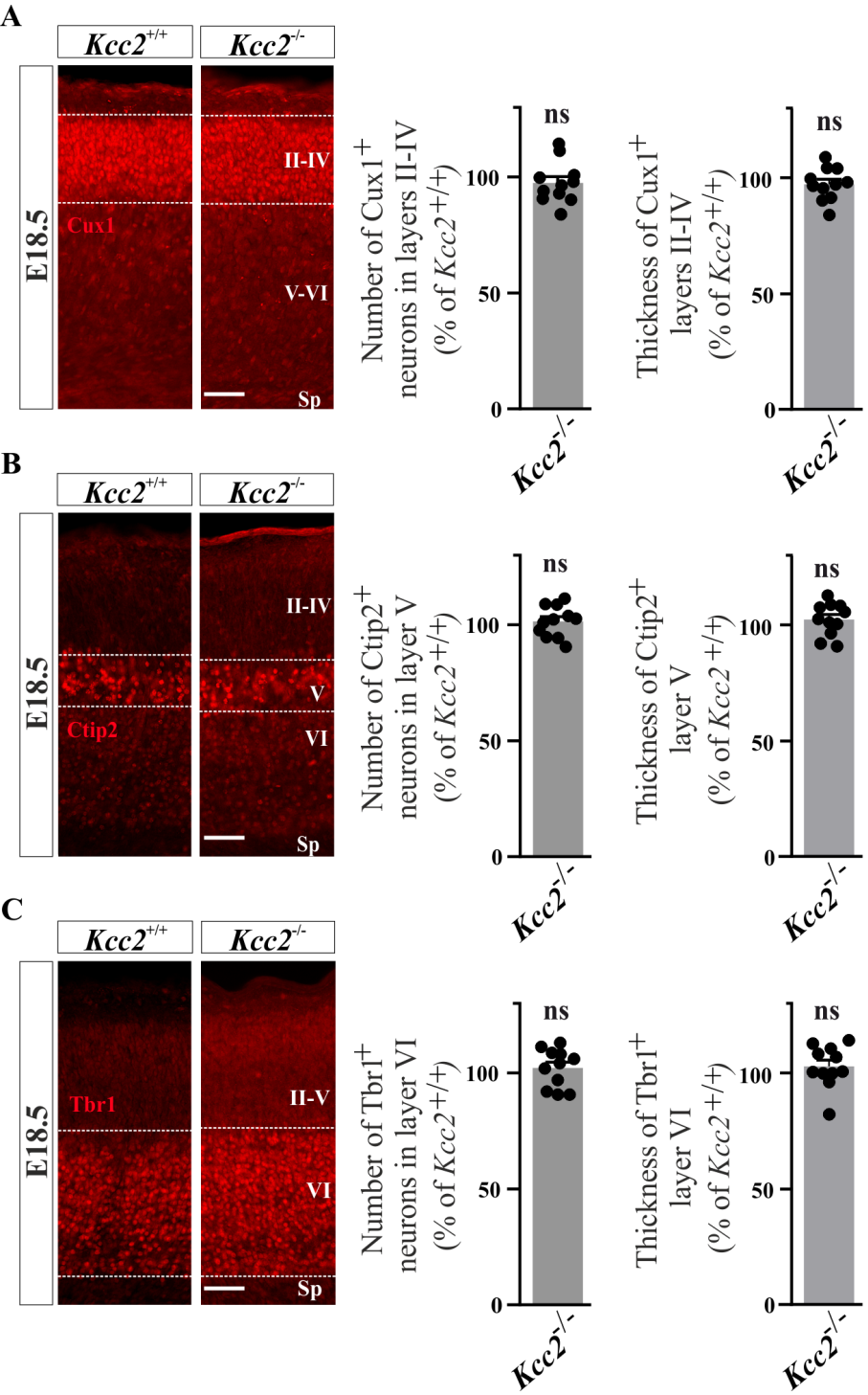
A
Kcc2+/+
Kcc2-/-
E18.5
Cux1
II-IV
V-VI
Sp
Number of Cux1+ neurons in layers II-IV (% of Kcc2+/+)
Thickness of Cux1+ layers II-IV (% of Kcc2+/+)
ns
100
50
0
Kcc2-/-
B
Ctip2
V
VI
Number of Ctip2+ neurons in layer V (% of Kcc2+/+)
Thickness of Ctip2+ layer V (% of Kcc2+/+)
C
Tbr1
II-V
Number of Tbr1+ neurons in layer VI (% of Kcc2+/+)
Thickness of Tbr1+ layer VI (% of Kcc2+/+)

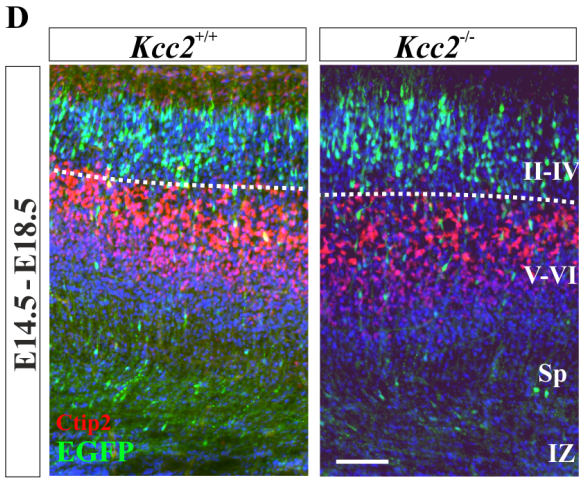
D
Kcc2+/+
Kcc2-/-
E14.5 - E18.5
II-IV
V-VI
Sp
IZ
Ctip2
EGFP

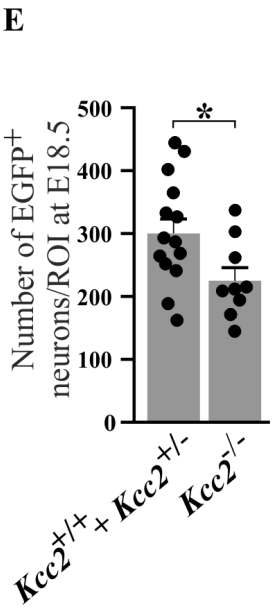
E
Number of EGFP+ neurons/ROI at E18.5
500
400
300
200
100
0
*
Kcc2+/+ + Kcc2+/-
Kcc2-/-

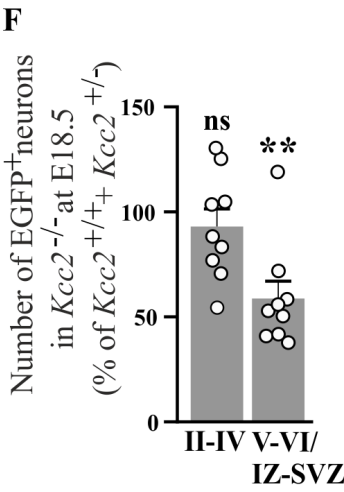
F
Number of EGFP+neurons in Kcc2-/- at E18.5 (% of Kcc2+/+ + Kcc2+/-)
150
100
50
0
ns
**
II-IV
V-VI/ IZ-SVZ

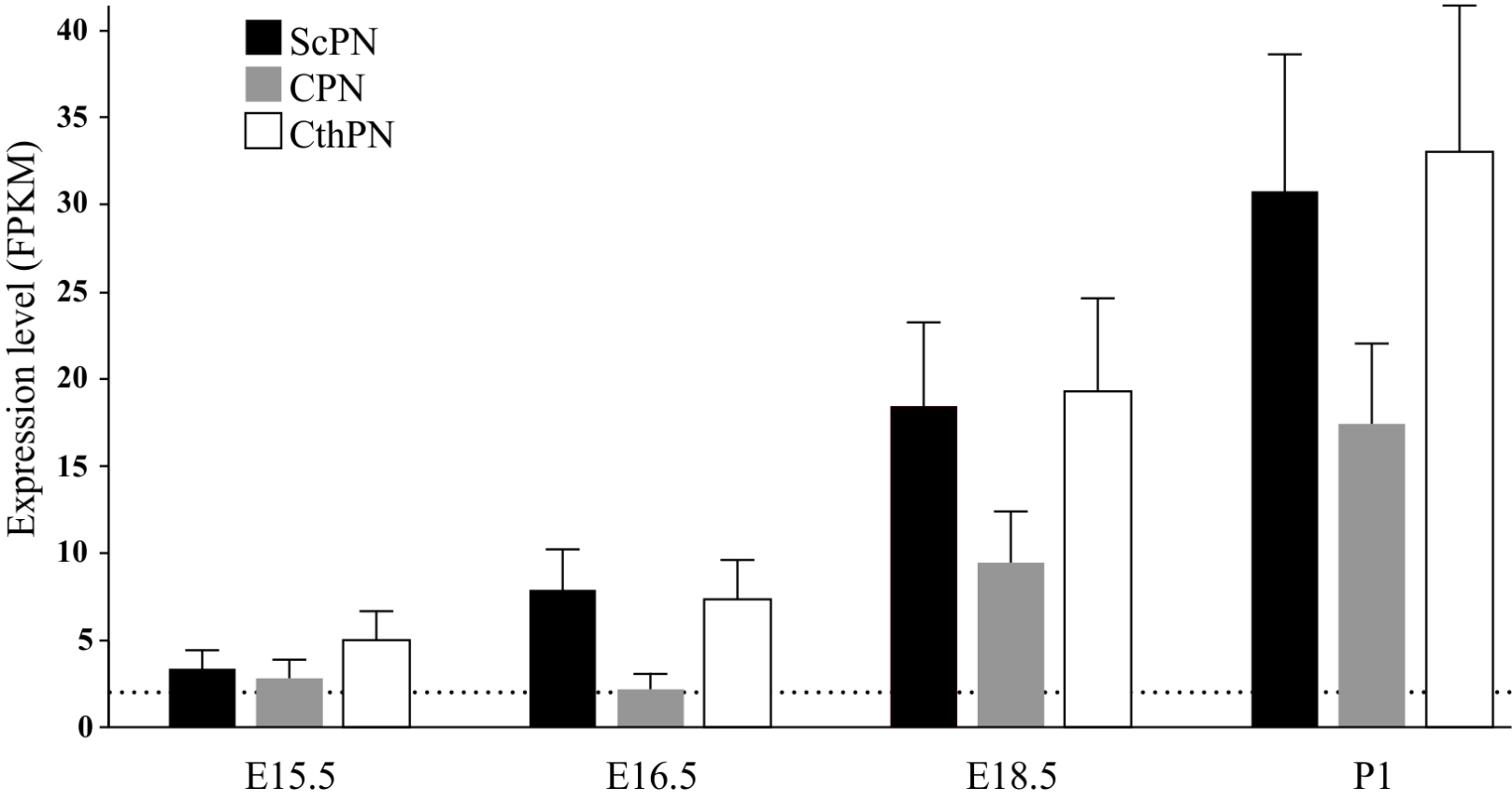
ScPN
CPN
CthPN
Expression level (FPKM)
40
35
30
25
20
15
10
5
0
E15.5
E16.5
E18.5
P1

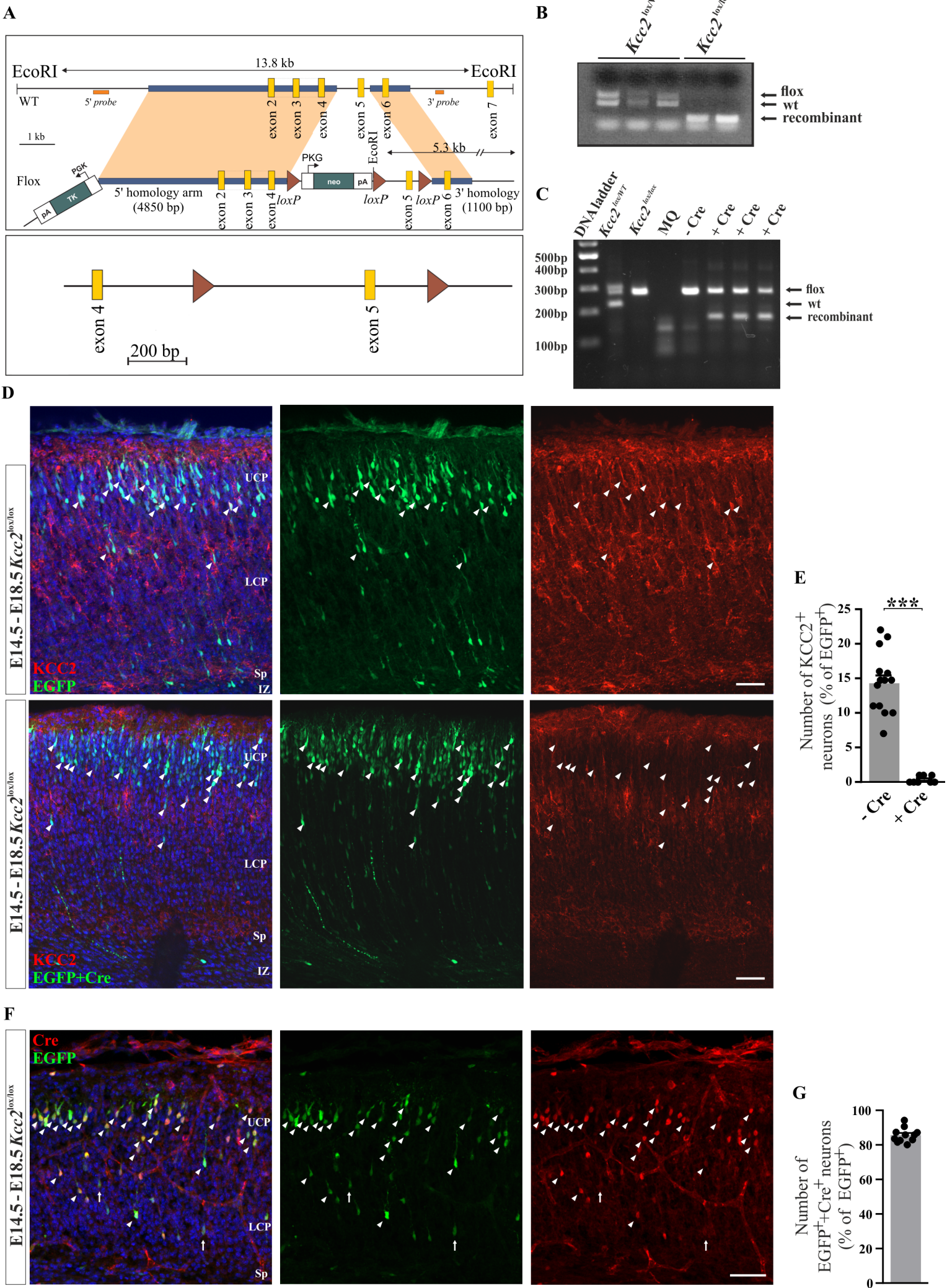
A
EcoRI
13.8 kb
EcoRI
WT
5' probe
3' probe
exon 2
exon 3
exon 4
exon 5
exon 6
exon 7
1 kb
5.3 kb
EcoRI
PKG
Flox
PGK
TK
pA
neo
pA
5' homology arm
(4850 bp)
loxP
loxP
loxP
3' homology
(1100 bp)
exon 4
exon 5
200 bp
B
Kcc2 lox/WT
Kcc2 lox/lox
flox
wt
recombinant
C
DNA ladder
Kcc2 lox/WT
Kcc2 lox/lox
MQ
- Cre
+ Cre
+ Cre
+ Cre
500bp
400bp
300bp
200bp
100bp
flox
wt
recombinant
D
E14.5 - E18.5 Kcc2 lox/lox
UCP
LCP
KCC2
EGFP
Sp
IZ
E14.5 - E18.5 Kcc2 lox/lox
UCP
LCP
KCC2
EGFP+Cre
Sp
IZ
E
***
Number of KCC2+ neurons (% of EGFP+)
25
20
15
10
5
0
- Cre
+ Cre
F
E14.5 - E18.5 Kcc2 lox/lox
Cre
EGFP
UCP
LCP
Sp
G
Number of EGFP+Cre+ neurons (% of EGFP+)
100
80
60
40
20
0

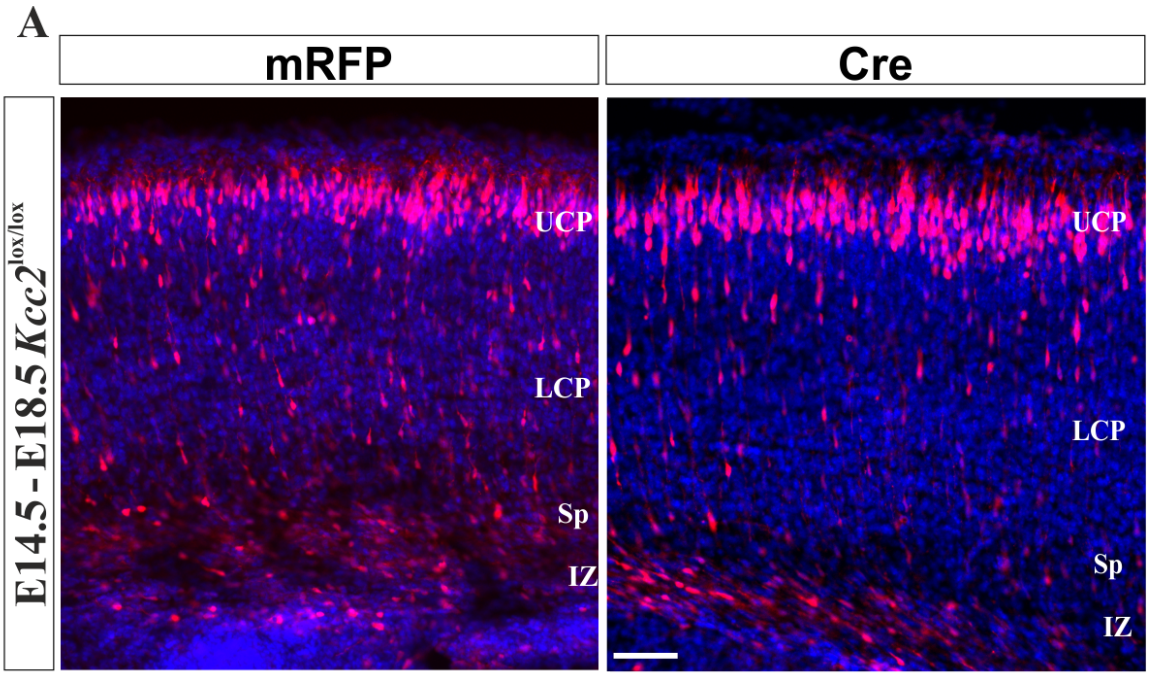
A
mRFP
Cre
E14.5 - E18.5 Kcc2lox/lox
UCP
LCP
Sp
IZ
UCP
LCP
Sp
IZ

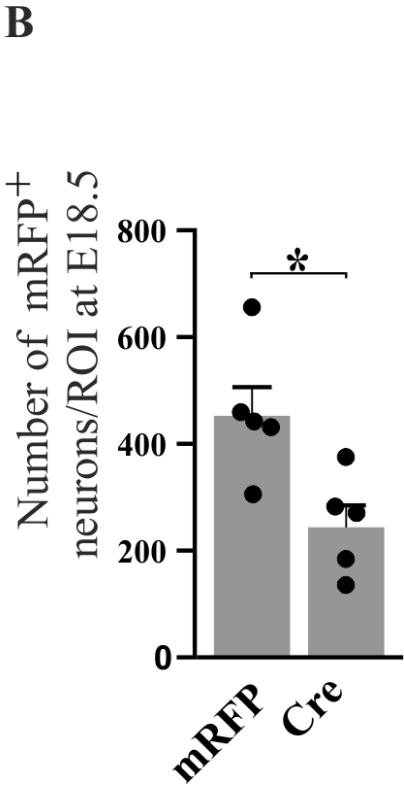
B
Number of mRFP+ neurons/ROI at E18.5
800
600
400
200
0
*
mRFP
Cre

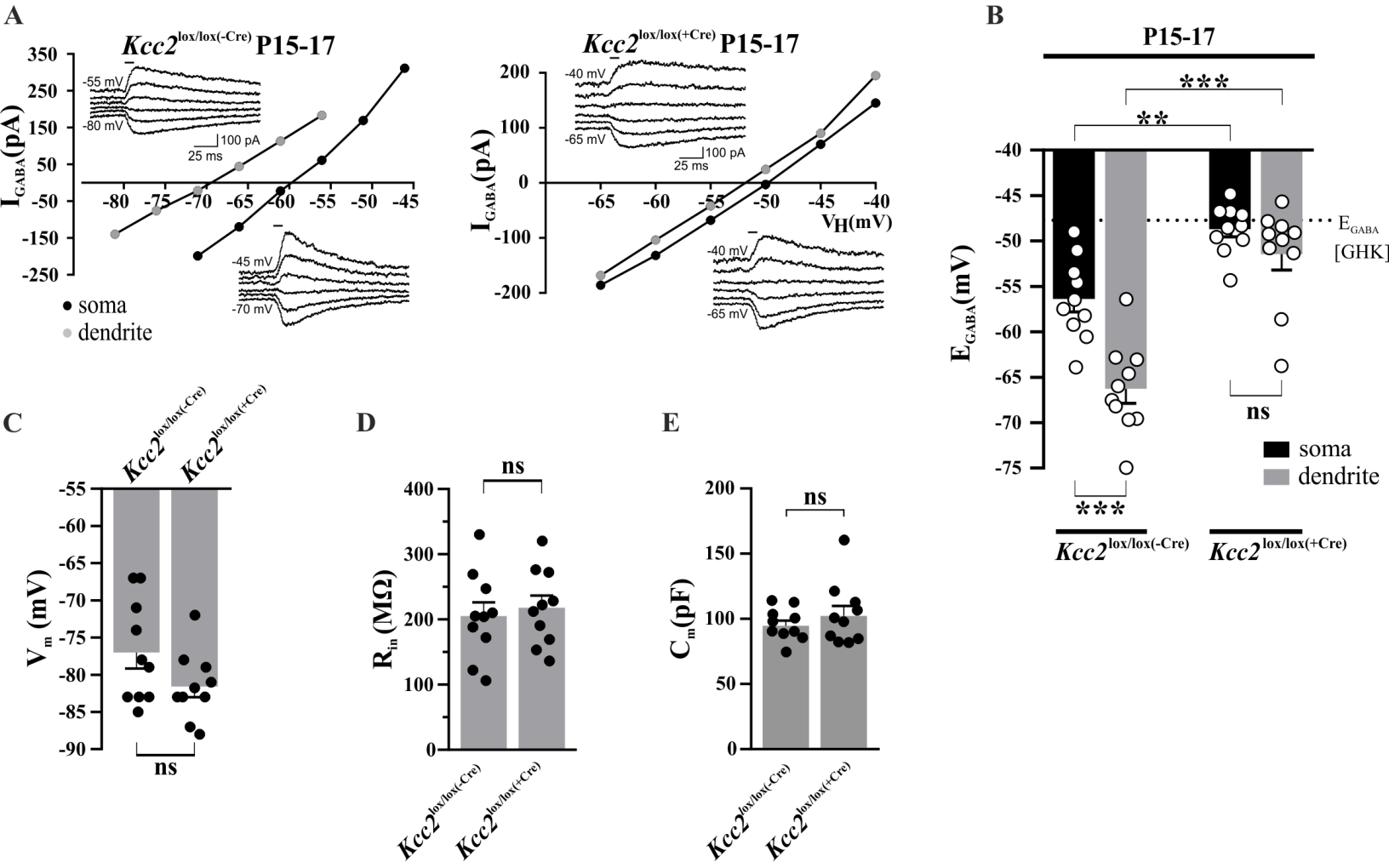
A
Kcc2lox/lox(-Cre) P15-17
Kcc2lox/lox(+Cre) P15-17
IGABA(pA)
VH(mV)
-55 mV
-80 mV
-45 mV
-70 mV
-40 mV
-65 mV
100 pA
25 ms
soma
dendrite
B
P15-17
EGABA (mV)
EGABA [GHK]
soma
dendrite
ns
***
**
Kcc2lox/lox(-Cre)
Kcc2lox/lox(+Cre)
C
Vm (mV)
ns
D
Rin (MΩ)
ns
E
Cm(pF)
ns